

Invited Review Article

A synthesis of the Peruvian Coastal Batholith: An exploration of temporal histories, causes of compositional diversity, and tectonomagmatic links in arcs

Ana María Martínez-Ardila^{a,*}, Lance Pompe^a, Benjamin L. Clausen^{a,b}, Scott R. Paterson^c, Gregory J. Holk^d, Peter Luffi^{e,f}

^a Department of Earth and Biological Sciences, Loma Linda University, Loma Linda, CA 92350, USA

^b Geoscience Research Institute, Loma Linda, CA 92350, USA
^c Claremont, CA 91711, USA

^d Department of Geological Sciences, California State University, Long Beach, CA 90840-3902, USA

^e Sabba Stefanescu Institute of Geodynamics, Bucharest, Romania

^f Geological Institute of Romania, Bucharest, Romania

ARTICLE INFO

Keywords:

Magmatic arcs
 Flare-ups
 Compositional diversity
 Geochemistry
 Geochronology
 Peruvian Coastal Batholith

ABSTRACT

The causes for spatial geochemical trends in the central Andes of Peru have been studied since the early 1970s. Along-arc chemical changes observed in the Peruvian Coastal Batholith (PCB) were fundamental to developing models for the evolution of the Pacific margin of South America. However, explanations for these trends and the processes that control magmatic compositional diversity along this arc are not fully understood. In this contribution we use an up-to-date database of high quality geochemical and geochronological data to: 1) assess the evidence for the previously proposed chemical trends, 2) document patterns of episodic magmatism to examine spatial and temporal changes covering a timespan of >170 million years along the PCB segments, 3) investigate PCB-wide variation of the parameters previously studied in the Ica-Pisco plutons, and 4) relate these to the tectonic setting, subduction parameters, magma sources, and crustal assimilation processes. Our results show that the PCB has a clear non-steady-state pattern over variable temporal and spatial scales and that arc magma chemistry covaries with arc magmatic activity. We conclude that the identified diversity in magma chemistry both along- and across-arc is the result of the extent of differentiation, types of assimilated materials, different types of basement, changes in crustal thickness, arc migration, changes in mantle input, and transitioning from depleted to lithospheric mantle resulting from changes in slab dip angle. In order to explain the causes of flare-ups and arc chemical diversity in the PCB we suggest that coupling of external (lower plate) and internal (upper plate) processes in complex ways at different spatial and temporal scales form the final arc diversity.

1. Introduction

The Peruvian Coastal Batholith (PCB) and associated volcanic rocks are the dominant features of Mesozoic arc magmatism in the Andes of Peru. It is located at the western margin of the Peruvian Andes and results from the Nazca plate subduction beneath the South American plate between 4° S at the Huancabamba deflection and 18° S (Fig. 1). The PCB is composed of >1000 plutonic bodies, cropping out over a 1600 km-long and 60 km-wide array. Along strike petrological trends in the PCB have been studied since the early 1970s and five distinct segments have been proposed from north to south: Piura, Trujillo, Lima, Arequipa, and

Toquepala (Fig. 1).

Along-arc chemical changes observed in the PCB were fundamental for developing models describing the evolution of the Pacific margin of South America (Castroviejo Bolibar et al., 2009; Dalmayrac et al., 1977; Fanlo et al., 2009; Rodrigues et al., 2010). Explanations for these trends initially included modification of the subduction style and parameters, changes in crustal thickness (Beckinsale et al., 1985; Boily et al., 1989; Cobbing and Pitcher, 1972; Mukasa, 1986), and pluton emplacement in different crustal domains (Mamani et al., 2010). The early understanding of the PCB has been extended by recent studies on structural style and orogenic evolution (Henrique-Pinto et al., 2021; Hildebrand and

* Corresponding author.

E-mail address: anmartinez@llu.edu (A.M. Martínez-Ardila).

<https://doi.org/10.1016/j.lithos.2023.107298>

Received 31 March 2023; Received in revised form 19 July 2023; Accepted 20 July 2023

Available online 22 July 2023

0024-4937/© 2023 The Authors. Published by Elsevier B.V. This is an open access article under the CC BY-NC-ND license (<http://creativecommons.org/licenses/by-nc-nd/4.0/>).

Whalen, 2014; Pfiffner and Gonzalez, 2013; Ramos, 2018), emplacement mechanisms and heat flow modeling (Gonzalez et al., 2020; Moore, 1984; Myers, 1975), and magma diversity as a result of the addition of subduction-related components to the mantle source, crustal assimilation, and magmatic recycling (Martínez Ardila et al., 2019a, 2019b). However, the timing of the magmatic events, the causes of the magmatic compositional diversity along the arc, and the precise geological history of the subduction-related magmatism are some of the questions that remain unanswered.

In this contribution we: 1) assess the evidence for the previously proposed along- and across-strike trends and evaluate magmatic processes by using an up-to-date database of high quality geochemical and geochronological data, 2) document patterns of episodic magmatism to examine spatial and temporal changes covering a timespan of >170 million years along the PCB segments, 3) compare PCB-wide variation of the same parameters previously studied in the Ica-Pisco plutons

(Martínez Ardila et al., 2019a, 2019b), and 4) focus on the tectonic setting, subduction parameters, magma sources, and crustal assimilation processes to explain the chemical and geochronological trends of the PCB. In addition, we use our geochemical and geochronological data to discuss some older concepts such as the superunit classification system, the relationships among plutons, the boundaries proposed for the mineralogical and chemical differences between segments, types of basement and accreted terrains, and problems associated with the scarcity of isotopic and radiometric data, especially in the northern segment, needed to establish its petrogenetic history.

2. Outstanding issues about the Evolution of Arcs

To understand better continental arcs and their evolution we must consider several topics such as the magma sources and mechanisms of compositional diversity, causes of flare-ups and lulls, spatial and

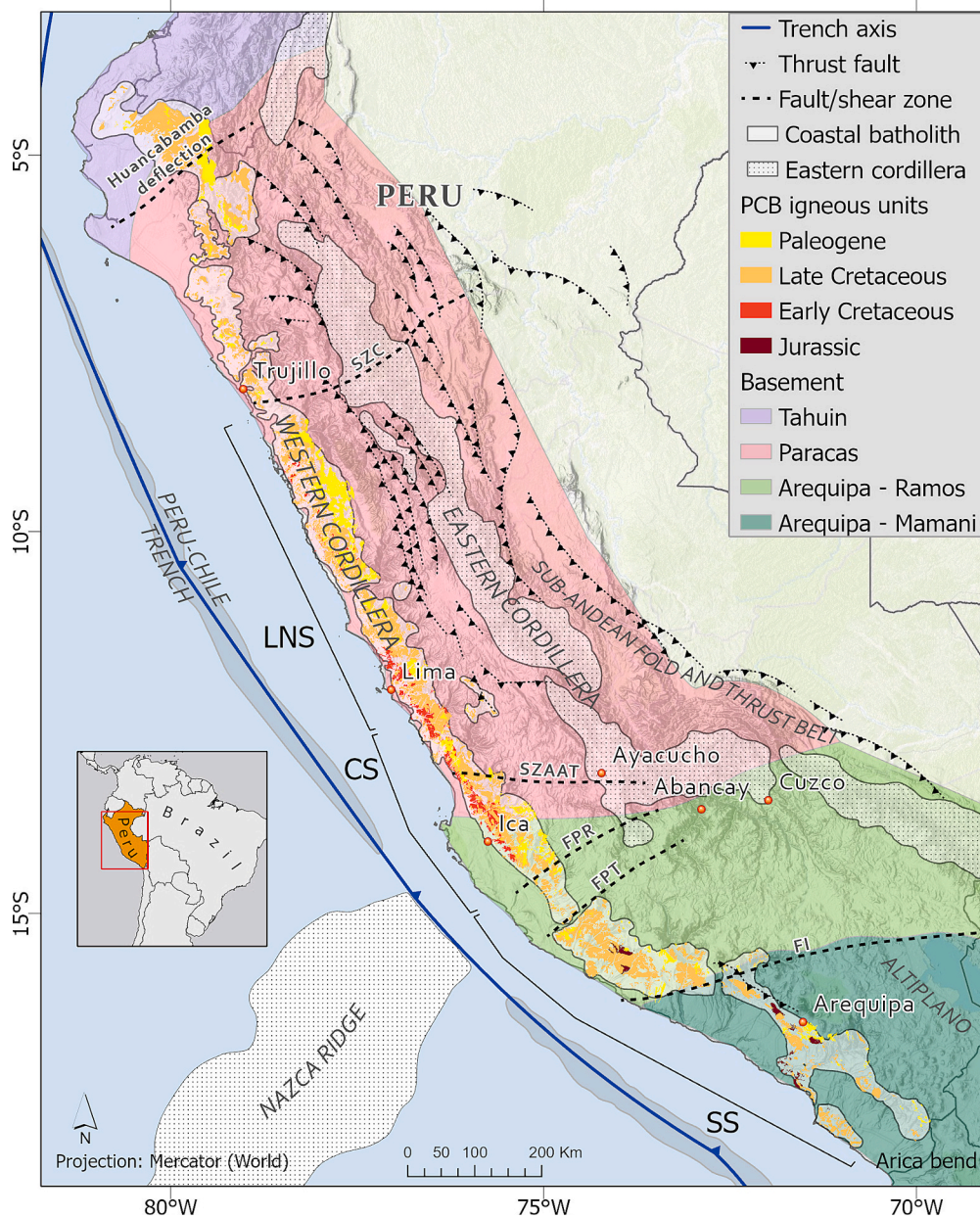


Fig. 1. Simplified geologic map of the Peruvian Coastal Batholith (PCB), crustal domains, and suggested segments. Lower North Segment (LNS), Central Transitional Segment (CS), and South Segment (SS). Patacancha-Tambuco Fault (FPT), Puyentimari Fault (FPR), Iquipi Fault (FI), Contaya Shear Zone (CSZ), Shear Zone Abancay-Andahuaylas (SZAAT).

temporal variations, and tectonic processes driving arc evolution. Geochemists and petrologists agree that magmatic rocks generated in subduction-related settings represent the end-product of a complex petrogenetic evolution involving multiple processes (e.g., partial melting, source contamination, crustal assimilation, magmatic mingling, mixing and recycling, and fractional crystallization) and variable contributions from depleted asthenospheric mantle, deep lithosphere, including the mantle lithosphere and lower crust, and a sedimentary component (Arndt and Goldstein, 1989; Ducea, 2001; Hildreth and Moorbath, 1988). The sedimentary component may be assimilated during magmatic differentiation and emplacement, may originate from subducted sediments or sedimentary rocks, or may be transported to the lower crust during shortening (Chapman et al., 2017). Also, changes in magma source compositions have been correlated with changes in tectonic processes which are necessary to drag crustal materials into the mantle (Castro et al., 2021; Castro et al., 2013). However, distinguishing and determining the exact proportions and mechanisms by which mantle- and crustal-derived components are involved in generating the compositional diversity of arc magmas remains challenging.

Continental arcs in the American Cordillera are characterized by patterns of episodic magmatism (de Silva et al., 2015; Kirsch et al., 2016; Paterson and Ducea, 2015). Episodicity may reflect a combination of internal feedback processes in the upper plate, mantle, or crust within the arc (Cao et al., 2016; Chin et al., 2015; DeCelles et al., 2009; DeCelles et al., 2015; Ducea, 2001), and/or external forcing by tectonic events outside the arc (de Silva et al., 2015; Hughes and Mahood, 2008; Zellmer, 2008). Linked geochemical, geochronological, and kinematic data sets from Cretaceous continental arcs suggest uncertain and variable correlations between flare-up events and convergence rates as well as with global events of plate tectonic reorganization (Kirsch et al., 2016). These observations support the idea that episodic mantle processes play the major role for triggering and driving continental arc flare-ups (Attia et al., 2020; Martínez Ardila et al., 2019a, 2019b; Schwartz et al., 2017).

Episodic arc magmatism and spatial and temporal variations (e.g., chemical trends, arc migration, and magmatic focusing) need further study to resolve or highlight the significance of chemical and isotopic changes related to different orogenic processes (de Silva and Gosnold, 2007; Hildreth and Moorbath, 1988; Lipman, 2007). A well-studied spatial trend is exemplified by the $^{87}\text{Sr}/^{86}\text{Sr}|_i$, ϵNd , and ϵHf isotopic trends in which the radiogenic isotopic composition of magmatism becomes increasingly evolved landward of the trench. A common interpretation of this isotopic variation indicates that the spatial isotopic trends may reflect crustal assimilation or mixing between depleted asthenospheric mantle and isotopically evolved continental lithospheric mantle and/or be associated with arc migration and/or changes in crustal thickness (Chapman et al., 2017; Kirsch et al., 2016).

3. Review of previous studies

Seventy years ago, Jenks and Harris (1953) published one of the first papers referring to the Peruvian Coastal Batholith, which provided the basis for understanding the nature and origin of the PCB. This preliminary work was followed by contributions from Harrison (1960), Bellido Bravo (1969), and Stewart and Garcia (1968) who studied the central zone of the batholith near Lima.

In 1965 a geological survey was begun by British and Peruvian geologists. It resulted in a number of outstanding papers focusing on the chronology, petrology, tectonic setting and structural complexity of the PCB, and it introduced the idea of dividing the batholith into five segments. In 1975 Myers published a paper presenting the cauldron subsidence model as an important emplacement mechanism and suggested a volcanic-plutonic link for the batholith. Bussell et al. (1976) supported Myers' ideas with data from four ring complexes he studied north of Lima. Cobbing et al. (1977) explained the segmentation of the PCB as the consequence of discontinuities in the subduction zone, with magmatism

in each segment possessing its own unique emplacement and spatial distribution. The same year, Dalmayrac et al. (1977) determined the first U—Pb ages from the Precambrian rocks of the southern Arequipa massif and distinguished it from the Paleozoic basement exposed in north and central Peru. He recognized the different basement rocks from north to south Peru and suggested that the Sr_i values and petrological changes along the length of the batholith were the result of magmas interacting with different types of basement.

A general summary of the segmented PCB and its geochemical character along with the associated volcanic rocks became available in 1979 when Atherton and Tarney edited a book, *Origin of Granite Batholiths: Geochemical Evidence*. The advance in understanding the PCB was complemented with new K—Ar, Rb—Sr, and U—Pb ages indicating that the igneous activity took place from Cretaceous to Paleocene (Beckinsale et al., 1985; Moore, 1984; Mukasa, 1984; Noble et al., 1978; Sanchez-Fernandez, 1982).

The 1965 survey, involving more than thirty British and Peruvian geologists, culminated in 1985 with the publication of the book *Magmatism at a Plate Edge: The Peruvian Andes* edited by Pitcher, Atherton, Cobbing and Beckinsale. This publication included a comprehensive review of the geological setting and pre-Mesozoic history of the Peruvian Andes, addressed the concept of units and superunits, emplacement mechanisms, structure and shape of the batholith, and origin of mineral deposits, and discussed the importance of the geochronology and geochemical characteristics in identifying the magma sources.

Motivated by ideas from Pitcher's book, new researchers became interested in studying the petrological changes along the PCB. Boily et al. (1989) presented a study of the chemical and isotopic evolution of the southern PCB indicating that the parental mafic magma(s) were derived from an isotopically depleted mantle wedge above the subduction zone and that magmas experienced crustal assimilation during ascent. In order to better explore the along-arc geochemical changes and their relationship to crustal changes, Atherton and Aguirre (1992) addressed the thermal and geotectonic setting of Cretaceous volcanic rocks in relation to Andean crustal thinning. They concluded that the source of the southern volcanic rocks was old enriched mantle beneath the Precambrian Arequipa Massif, in contrast to the mantle beneath central Peru which they considered to be much younger and less enriched.

Several models were suggested to explain the mineralogical and chemical differences between the PCB segments, but it was not until after 2000 that evidence supporting the accretion of parautochthonous Paracas and allochthonous Arequipa continental terrains was linked to the geochemical changes observed in the PCB (Mamani et al., 2008; Ramos, 2018; Rodrigues et al., 2010 and Willner et al., 2014). The chemistry of the northern segment was explained as resulting from accreted terrains and the development of a rift zone with back arc basins and volcanic arcs (Rodríguez Morante and Huanacuni Mamani, 2011). Plutons emplaced in the central segment intruded an oceanic crust of Permian-Triassic age developed by attenuation of the preexisting continental crust (Bahlburg et al., 2006; De Haller et al., 2006; Polliand et al., 2005; Ramos and Alemán, 2000). Carlotto et al. (2009) suggested that the emplacement mechanisms in the central segment were associated with the Ica, Tapacocha-Conchao-Cocachacra fault systems and plutons in this area interacted with Jurassic and Lower Cretaceous volcano-sedimentary units. On the other hand, the southern segment is influenced by the rise of magmas through thicker Precambrian and Paleozoic basement with evidence of higher crustal contamination than the other segments (Moore and Agar, 1985; Boily et al., 1989).

The most recent publications dealing with the magmatic history of the PCB include the studies developed by Martínez Ardila et al. (2019a, 2019b) and Ccallo Morocco et al. (2021). The first study included field, petrographic, geochronological, and geochemical data to unravel magma sources. It concluded that the PCB composition in the Ica-Pisco area was derived from magmas made up of approximately 65–70% mantle, 20–25% mantle source contamination from an isotopically

evolved subduction component dominated by Pacific Ocean sediments, and 5–10% assimilated and recycled crustal materials. The second publication reported new geochemistry and U–Pb ages from plutons in the central segment. It was conducted within the framework of a geological survey developed by the Geological Mining and Metallurgical Institute (INGEMMET) of Peru and the China Geological Survey (CGS) between the years 2017 and 2018.

3.1. Geologic overview

The Peruvian Andes (Fig. 1), located between 4° S (the Huanca-bamba deflection) and 18° S (the Arica deflection, or Bolivian orocline), are made up of six linear geological provinces parallel to the Pacific coast (Dunbar et al., 1990; Jaillard et al., 2000; Sébrier et al., 1988; Wipf, 2006). From west to east, these are (1) Coastal Forearc, (2) Western Cordillera, (3) Altiplano, (4) Eastern Cordillera, (5) Sub-Andean Fold and Thrust Belt, and (6) Foreland Basin.

The Coastal Batholith, which is the focus of this paper, dominates the Western Cordillera. It represents a linear belt of calc-alkaline granitoids ranging from Lower Jurassic to Upper Eocene (Hildebrand and Whalen, 2014; Mukasa, 1986; Pitcher et al., 1985). In the Western Cordillera, stratigraphically and structurally continuous basins are considered to be part of a marginal basin that encompassed all of the West Peruvian Trough (Atherton et al., 1985; Cobbing, 1978). The major interconnected basins are Huarmey in the north and Rio Cañete to the south, both of which were filled with 5–9 km of Cretaceous, Tithonian-Albian, submarine basaltic, andesitic, and dacitic volcanic rocks, referred to as the Casma Group (Cobbing, 1978, 1985). It is assumed that the rocks of the Huarmey-Cañete basins were intruded by the early plutons of the Coastal batholith (Atherton et al., 1983; Atherton et al., 1985; Cobbing et al., 1977; De Haller et al., 2006; Myers, 1975). The basement for the Huarmey-Cañete Trough and the Coastal batholith in the south is the Mesoproterozoic Arequipa terrane (Casquet et al., 2010; Loewy et al., 2004; Shackleton et al., 1979). To the north, there are no exposures of the Neoproterozoic to Paleozoic basement of the Arequipa-Paracas terrane on land; however, recent exploration wells and studies of offshore islands identified Precambrian basement underlying the Paracas terrane (Romero et al., 2013). The youngest units in the Western Cordillera correspond to remnants of several units of Cenozoic volcanic and volcanoclastic rocks that cap the Western Cordillera. These rocks range in age from at least Eocene to Quaternary and the older units show the effects of contractional deformation (Wipf, 2006).

3.2. Old paradigms of the architecture and structural framework

The PCB is made up of more than a thousand plutons in a belt that runs subparallel to the coast, extends for 1600 km, and is up to 80 km across (Fig. 1). The batholith is described as a series of Mesozoic-Tertiary plutons, mostly classified as diorite, tonalite, granodiorite, and monzogranite. These plutons were emplaced at high crustal levels through a combination of roof-lifting and cauldron subsidence forming nested plutons and dike swarms (Haederle and Atherton, 2002; Mukasa, 1986; Myers, 1975; Pitcher et al., 1985). This area is one of the first places where cauldron subsidence was considered an important emplacement mechanism (Myers, 1975). Their interpretation was based on apparent weak, structural and thermal pluton aureoles, the lack of physical disruption of the volcanic host rock, the geometry of the typically tabular plutons with Andean-trending, assumed fault-controlled contacts, and ring dikes and nested plutons with steeply dipping sides and flat roofs (Bussell et al., 1976; Agar, 1978; Moore, 1979; Pitcher et al., 1985). Bussell and Pitcher (1985) suggested the dike swarm and nested pluton (with younger ages towards the center) shapes as evidence of batholith-normal extension during emplacement and that the magmas rose everywhere to a similarly high subvolcanic level in the crust independent of the time of emplacement. Haederle and Atherton (2002) also suggested that the melts ascended up dike-like conduits to within 2

to 3 km of the surface, then spread laterally to form tabular plutons. Other authors like Wise (2002) and Polliard et al. (2005) favored several emplacement mechanisms including strike-slip control developed by contractional stresses and suggested a correlation between magmatism and strike-slip faulting.

3.3. Tectonic evolution of Western Peru

The tectonic history of Peru over the Phanerozoic was one of continuous eastward subduction of the Nazca and precursor Farallon oceanic plate beneath the continental South American plate (Miskovic et al. Ramos, 2009). Jaillard and Soler (1996) concluded that over the past ~200 Ma the tectonic evolution of the central and southern PCB is defined by short-lived contractional and extensional tectonic events controlled by changes in convergence rate and/or direction. Jaillard and Soler (1996) also suggested that major periods of shortening correspond to times of relatively fast convergence rates, while periods of extension are marked by relatively slow convergence rates. They based the convergence rates on global spreading rates and the contraction/extension and subsidence on stratigraphic analysis of two W-E transects in the north and south of Peru. Over time, the magmatic arc migrates towards the east. This has been explained by a decrease in dip angle, which would result in subduction erosion and subsidence of the forearc (Jaillard and Soler, 1996).

The tectono-magmatic history of the PCB as discussed by several authors (Espurt et al., 2008; Jaillard and Soler, 1996; Pardo-Casas and Molnar, 1987; Sdrolias and Müller, 2006; Soler and Bonhomme, 1990) has been divided into four main stages illustrated in Fig. 2 and summarized below.

The Jurassic-Early Cretaceous stage (~200 to 140 Ma) from Late Jurassic to Berriasian has been associated with a transtensional to extensional regime (Kay et al., 1999; Ramos, 1999) in the arc controlled by the absolute motion of the upper plate when Gondwana moved to the east, the Farallon plate convergence direction towards the N, with decoupling in the plates, and the trench rollback produced extension in the upper plate (Daly, 1989; Ramos, 1999; Ramos and Alemán, 2000). The period of extension in the back arc at the same time is related to the break-up of Gondwana and to the Tethyan rifting. The extension is attributed to a global change in plate kinematics (Ramos and Alemán, 2000; Ramos, 2010) characterized by large-scale marine transgressions and scarce juvenile arc magmatism in intra-arc basins up to 9 km thick along the continental margin (Romero et al., 2013; Sempere et al., 2002). In northern Peru, the activity of the continental volcanic arc ceased by the end of Kimmeridgian times (~150 to 140 Ma ago, Aspdén et al., 1987; Mourier, 1988; Litherland, 1994). In the back-arc areas of central Peru, scattered lava flows interbedded in Early Liassic marine sediments display alkaline chemistry, indicating that an extensional tectonic regime still prevailed in the back-arc (Regan, 1985; Romeuf et al., 1997). At the same time in southern Peru abundant arc magmatism, a rapidly evolving tectonic regime, subaerial back-arc sedimentation and local marine fore-arc deposits prevailed (Jaillard et al., 2000). These features are attributed to a steeply dipping slab, a slow oblique convergence rate, and a thin continental crust.

The Early Cretaceous stage (~140 to 100 Ma) marks the onset of the Andean orogeny characterized by the transition from an extensional to a weak contractional setting due to a complete reorganization of the paleographic pattern and tectonic evolution of the Andean margin (Ramos and Alemán, 2000). The deformed and eroded magmatic arc is then overlain by unconformable Valanginian (?) to Albian fluvio-marine deposits and the creation of a N-S trending pull-apart basin (Villagomez et al., 1996). This unconformity suggests the occurrence of a significant latest Jurassic-Early Cretaceous tectonic event (Litherland, 1994). Volcanic arc activity in central Peru continued during part of the Berriasian times. In central and southern Peru, scarce outcrops of volcanic rocks in the coastal and western areas suggest that volcanic arc activity continued at least locally until Aptian times (Bellido Bravo, 1969; Vidal

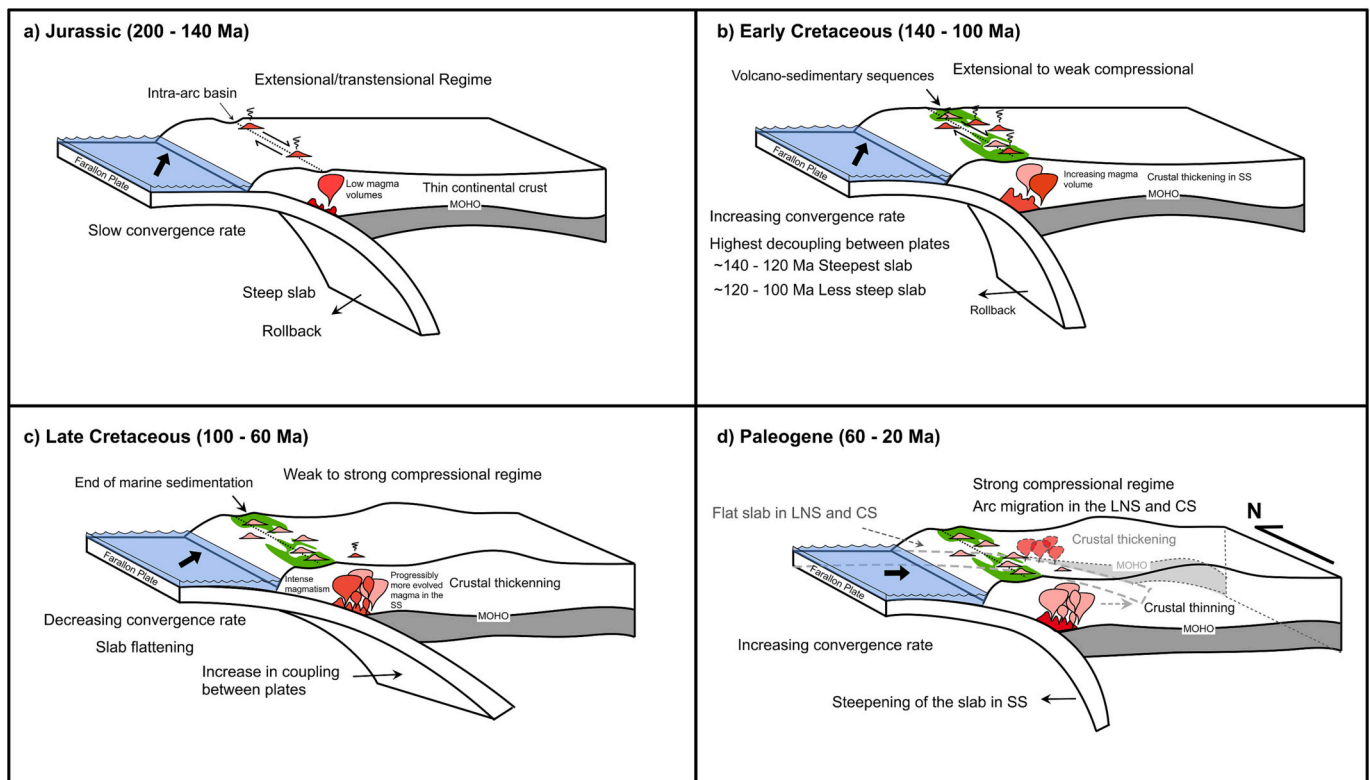


Fig. 2. Tectono-magmatic Evolution of Western Peru. (a) Jurassic stage (~200–140 Ma): transensional to extensional regime controlled by the absolute motion of the upper plate, slow convergence rate and reduced magmatism. (b) Early Cretaceous stage (~140–100 Ma): transition from an extensional to a weak compressional, the onset of the Andean orogeny with increasing magmatism, and marked by marine transgressions. (c) Late Cretaceous stage (~100–60 Ma) represent the transition from weak compressional to a strong compressional setting with decreasing convergence rates, slab flattening, increasing plate coupling, and intense magmatism. (d) Paleogene stage (60–20 Ma) characterized by increasing convergence rates, strong compressional regime, low magmatism and contrasting behavior between northern (flat slab, crustal thinning) and southern (steepening slab, crustal thickening) Peru.

C et al., 1990). During the early Albian a multistage, extensional to transensional subduction setting is characterized by (1) a calc-alkaline volcanic arc marked by a marine transgression culminating in the late Albian or early Cenomanian. (2) The intense volcanic activity in the magmatic arc and the beginning of upper-crustal magmatic intrusions. (3) Early Cretaceous plutons intruded folded Jurassic to Early Cretaceous volcanoclastics, indicating a contractional phase in the Early Cretaceous. In northern Peru, the NW trending magmatic arc in the Late Tithonian represents evidence for a drastic change in the convergence direction towards NE. During this phase, a change from a slow to fast convergence rate occurs (2–15 cm/yr) (Jaillard and Soler, 1996; Soler and Bonhomme, 1990).

A Late Cretaceous stage is characterized by the transition from a weak to strong contractional setting starting at ~100 Ma. This is marked by local folding and faulting, the end of marine sedimentation, and intense magmatic activity (Soler and Bonhomme, 1990). The contractional setting led to the emplacement of the bulk of the PCB between about ~100 Ma and 60 Ma (Hildebrand and Whalen, 2014; Mukasa, 1986; Pitcher et al., 1985). The change from marine sedimentation of the Jurassic and Early Cretaceous to continental sedimentation in the Late Cretaceous documents uplift, which is thought to be caused by contraction. The early Coniacian was characterized by a strong contractional tectonic regime, a progressive change of slab dip from $\pm 45^\circ$ to $\pm 30^\circ$, and changes in convergence rates from slow to rapid to slow again (65–55 Ma: 5–7 cm/yr; 50–37 Ma: >10 cm/yr; 36–25 Ma: ~5 cm/yr). Crust continues to thicken due to tectonic shortening, causing extensive folding and reverse faulting (Dalmayrac et al., 1977; Pffiffer and Gonzalez, 2013). This phase is marked by shallowing subduction angle with variable changes in convergence rate (Mégard, 1984; Pardo-Casas and Molnar, 1987; Ramos and Alemán, 2000; Soler and

Bonhomme, 1990). During this phase, large volumes of volcanic and plutonic rocks were emplaced all along the Peruvian margin (Jaillard et al., 2000).

The final stage starts in the Paleogene and is characterized by a strong contractional regime, a relatively flat slab dip of 30° for north and central Peru, but steeper subduction at $\sim 40^\circ$ in southern Peru. At ~24 Ma the convergence rate is rapid again (>10 cm/yr). A change in convergence direction from N to NE occurred in the Paleocene with a fast pulse in the Eocene between 55 and 40 Ma (Sdrolia and Müller, 2006). The major Late Eocene shortening phase is marked by a significant eastward shift of the magmatic front and migration of the arc (Jaillard and Soler, 1996). The magmatic belt records no changes in subduction parameters until the end of the magmatic activity in central Peru at ~3 Ma.

High rates of tectonic erosion of the overriding plate and the end of volcanism in central Peru have been linked to a low subduction angle related to the subduction of the Nazca ridge (Gutscher, 2002). In the Andes, the variation in the angle of subduction between the different segments is attributed to changes in slab buoyancy. Flattening due to the effect of the collision of aseismic ridges or steepening caused by the displacement towards the south of the collision zone (Ramos and Folguera, 2005).

The link between magmatism and tectonic settings and subduction parameters in the Andes have been discussed by several authors. For example, Bussell and Pitcher (1985) concluded that periods of rapid convergence coincided with enhanced PCB magmatic activity and suggested a relationship between the time of magmatic pulses and the concurrent relative plate motion between the South American and Nazca plates. However, other authors have found that the magmatic pulses are not always directly linked to contractional deformation events

and that the emplacement of the PCB took place during slow convergence (Jaillard and Soler, 1996; Soler and Bonhomme, 1990). More recently, Jaillard et al. (2000), Pfiffner and Gonzalez (2013), and Kirsch et al. (2016) presented evidence that the PCB magmatic pulses are not directly linked to contractional deformation events nor known subduction parameters.

3.4. The PCB basement

A study of tectonic events affecting the continental margin of Peru suggests a strong influence from the Precambrian Arequipa and Paracas terranes that collided with the Amazonian craton (Carlotto et al., 2009; Mišković et al., 2009; Ramos, 2009; Ramos, 2018), as well as subsequent contrasting Paleozoic evolution (Fig. 1).

The Arequipa allochthonous terrane was first recognized by Dalmayrac et al. (1977, 1980). Seismological studies of Dorbath (1996) together with the gravimetric, geochemical, and isotopic analyses of Mamani-Huisa (2006) and Mamani et al. (2008, 2010) outlined the extent of this cratonic block. A consensus finds that the Arequipa Massif, as part of the Arequipa terrane with a protolith age of ~2000 Ma, was first accreted in the late Mesoproterozoic during the amalgamation of the Rodinia supercontinent (Loewy et al., 2004; Reimann et al., 2010). During the Ordovician it was reactivated, when a back-arc basin formed along the old Mesoproterozoic suture (Díaz-Martínez et al., 2001; Sempere et al., 2008). This weak suture zone accompanied the emplacement of Late Paleozoic and Oligocene-Early Miocene granites during extensional regimes, and even controlled the crustal delamination at late Cenozoic times (Beck and Zandt, 2002; Jiménez and López-Velásquez, 2008).

In central Peru, the story is different for the 1158 Ma parautochthonous Paracas terrane (Keppie and Ortega-Gutiérrez, 2010). The Paracas block collided during Early Ordovician against Gondwana at ~465 Ma and reactivated during Eopaleozoic extension that reopened the old suture to form oceanic crust between Amazonia and Paracas (Ramos, 2008). The subduction of this oceanic crust developed a magmatic arc which is preserved in the Eastern Cordillera of Peru. The presence of a cratonic block underlying the Western Cordillera and adjacent offshore was demonstrated by the studies of Romero Fernández et al. (2011), who confirmed a Precambrian basement underlying the Paracas terrane. Romero et al. (2013) and Ramos (2018) suggested that large parts of this basement have been eroded away by subduction erosion. During most of the Jurassic an extensional regime dominated the western margin of Peru and developed rift basins in the hanging-wall of the terrane sutures. The Peruvian Late Cretaceous orogeny produced the emplacement of the Coastal batholith, the beginning of deformation along the coast, and the first foreland basins.

The Arequipa and Paracas terranes are the most studied areas of the pre-PCB basement. In contrast, the Tahuín basement in the northwest region lacks geophysical, geochemical, and geochronological studies leading to disagreement about its tectonic evolution. This block was considered by Feininger (1987) and Mpodozis and Ramos (1989) as an allochthonous Paleozoic terrane accreted during Cretaceous times, based on the comparison with the Paleozoic sequences exposed in southern Ecuador and on paleomagnetic data. Another interpretation, based on the U/Pb and Ar—Ar dating of metamorphic rocks, suggests that the Tahuín terrane collided against the Gondwana margin during the Alleghanian orogeny, possibly as a part of Laurentia, and it was left on the Gondwana margin after being detached from Laurentia (Cardona et al., 2005; Ramos, 2009). Other authors interpreted the Tahuín terrane as an autochthonous part of Gondwana (Bellido et al., 2009; Timoteo et al., 2012). New studies by Witt et al. (2017) in the Tahuín terrane indicate that this block collided against the Gondwana margin in the Early Permian after the docking of the Paracas terrane.

An understanding of the nature and evolution of the pre-PCB basement is still controversial, in spite of contributions from previous researchers. Therefore, one objective of this paper is to provide new data

to identify magma sources, the role played by the different types of basement, and their direct relationship with the mechanisms of compositional diversity for the central and southern segments.

3.5. Segmentation and superunits of the PCB

The south-to-north and west-to-east chemical variation of the PCB encouraged Cobbing and Pitcher (1983) to group the intrusive units within segments using the concept of “superunit”. As a result, five distinct segments were proposed on the basis of compositional differences and named, from south to north: Toquepala (18–16.5°S), Arequipa (16.5–12°S), Lima (12–9°S), Trujillo (9–6.5°S), and Piura (6.5–4°S) (Cobbing and Pitcher, 1972; Taylor, 1973; Regan, 1976; Cobbing et al., 1977; Cobbing and Pitcher, 1983).

The superunit concept was intended to identify distinct periods of magmatic activity characterized by distinct histories. This concept was used to infer a close genetic connection between all plutons within a superunit, which has some regional support from the detailed geochemical studies. However, this grouping system relied on poorly dated units resulting in disagreements about names of units (e.g., Instituto Geológico Minero y Metalúrgico Bulletins; Tosdal et al., 1981; Kaneoka and Guevara, 1984; Ellison et al., 1989; Mukasa, 1986; Mukasa, 1986; Clark et al., 1990; Quang et al., 2005). Also, dating from the various segments of the batholith demonstrated that plutons within individual proposed superunits were not always contemporaneous (Martínez Ardila et al., 2019a, 2019b; Moore and Agar, 1985; Mukasa, 1986). Despite the problems associated with the concept of superunits, this classification system continues to be used today to facilitate comparisons.

Recently, Ccallo Morocco et al. (2021) suggested reducing the previously proposed 5 PCB segments to only three: Piura (4–6°S), Lima (6–14.5°S), and Arequipa (14.5–18°S) and two transition zones between segments: Trujillo-Chiclayo (6–8.5°S) and Chaparra-Caraveli (14.5–16°S). The boundaries between PCB segments coincide with ancient fault zones where rifting during the Permo-Triassic and the Jurassic controlled basin formation, magmatism, and mineralization (Carlotto et al., 2009). For example, the boundary between the Piura and Trujillo segments is the Huancabamba deflection, a major oroclinal bend (Mitouard et al., 1990; Mourier, 1988). The boundary between the Trujillo and Lima segments is defined by NW-SE faults of the Contaya shear zone (Carlotto et al., 2009; Zelasco, 2011). The boundary between Lima and Arequipa segments is defined by the NW-SE Iquipi fault system.

4. Synthesis of datasets

4.1. Geochronology data

The available geochronological data for the PCB were obtained from K—Ar isochron ages on hornblende and biotite (Clark et al., 1990; Litherland, 1994; Martínez Valladares and Cervantes Gárate, 2003; Moore, 1984; Stewart et al., 1974), Rb—Sr whole rock isochron ages (Beckinsale et al., 1985; Sanchez-Fernandez, 1982), U—Pb whole rock (bulk zircon) ages (Mukasa, 1986), and U—Pb zircon ages (Ccallo Morocco et al., 2021; Martínez Ardila et al., 2019a, 2019b and Santos et al., 2016). These methods all have limitations: (1) K—Ar ages are often cooling and/or reheating ages and don't necessarily provide information on original pluton crystallization times; (2) Rb—Sr ages may represent mixed isochrons of different minerals derived from different magmas; (3) Rb—Sr ages are greatly affected by hydrothermal processes; and (4) many of the early U—Pb zircon ages were whole-rock, multi-grain zircon ages that average different zircon populations from a single sample.

The available geochronological data from igneous units (Supplementary Data) supports the idea that the PCB was constructed by several magmatic pulses during the north-eastward migration of the arc from

~200 to 20 Ma (Fig. 3). In addition, Martínez Ardila et al. (2019a, 2019b) and Voos et al. (2021) used U–Pb zircon ages to document three flare-ups (Fig. 3b) for the central transitional segment over 80 m.y.: (1) ~136–126 Ma, (2) ~120–80 Ma, and (3) ~70–56 Ma, younging towards the north-east. These ages were compared to ages found in the north segment, 100–95, 95–90, 90–70, and 70–50 Ma (Bussell and Pitcher, 1985; Myers, 1975), and suggested a synchrony of the described younger flare-ups along the two arc segments (Martínez Ardila et al., 2019a, 2019b).

4.1.1. Synthesis and new ages

To supplement the available geochronological data for the PCB, we present 29 new U–Pb single zircon ages from plutonic samples obtained at the University of Arizona Laserchron Center. Measured 20 μm beam spots included cores and rims when textural complexity was identified in the zircons. Most of the U–Th/Pb isotopic measurements were performed by Element 2 single-collector laser ablation-inductively coupled plasma mass spectrometry (LA-ICP-MS) followed the procedure outlined by Gehrels et al. (2008) and Johnston et al. (2009). Final ages reported and discussed throughout this paper are concordia ages calculated using the Isoplot Excel® macro of Ludwig (2003). Ages given in the text and figures are quoted at a 2σ confidence level. All geochronological data are included in supplementary material, and errors are reported at $\pm 2\sigma$ (see the

Supplementary Data).

4.2. Petrology and geochemistry

Previously recognized along-arc chemical trends from south to central Peru include decreasing K_2O (Cobbing, 1985) and Sr_i values (Beckinsale et al., 1985; Boily et al., 1989; Winter, 2008) and increasing $^{206}\text{Pb}/^{204}\text{Pb}$ isotope ratios (Mukasa, 1984). For example, it is suggested that in the southern segment the rise of magmas through thicker Precambrian and Paleozoic basement of the Arequipa terrane (Couch et al., 1981; Jones, 1981) results in higher crustal contamination indicated by more evolved Sr_i and Pb isotope data (Beckinsale et al., 1985; Boily et al., 1989 and Mukasa, 1986). The central segment is characterized by a larger proportion of gabbro, with most gabbro plutons occurring along the western flank, and by a diversity of more siliceous rocks including quartz diorite, tonalite, granite, and monzogranite (Regan, 1985), all with primitive isotope ratios (Beckinsale et al., 1985; Boily et al., 1989; Martínez Ardila et al., 2019a, 2019b; Mukasa, 1986). More limited contamination in the central segment has been explained as the result of magmas interacting with a different type of basement, in this case the Mesoproterozoic Paracas terrane (Mamani et al., 2010; Petford and Atherton, 1995).

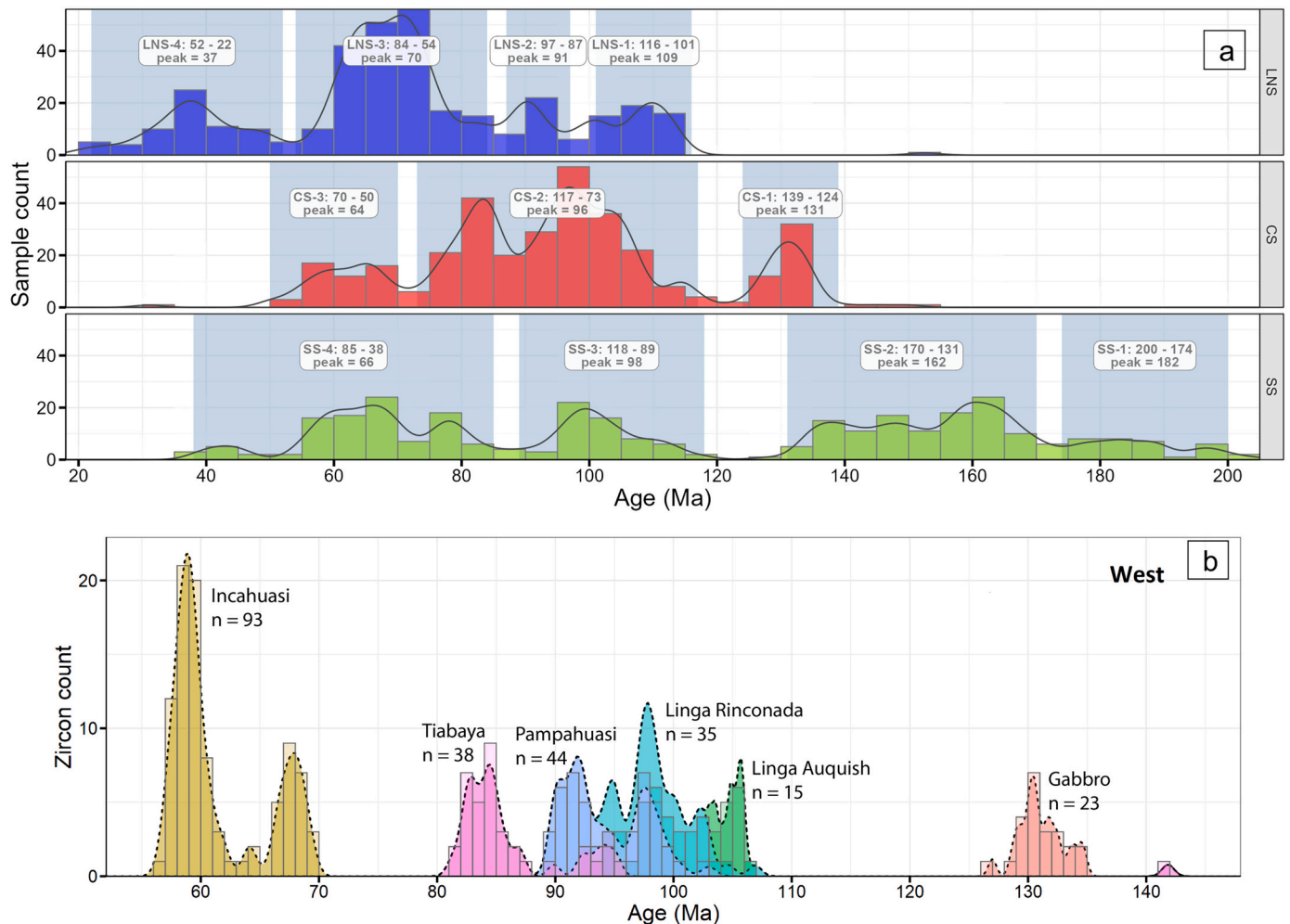


Fig. 3. a. Igneous bedrock age spectra histogram and kernel density estimation depicting flare-ups across the Lower North Segment (LNS), Central Transitional Segment (CS), and South Segment (SS). The sample ages are a combination of measured U–Pb ages and geochemistry samples that have K–Ar, Rb–Sr, Ar–Ar, and estimated ages. Age data are smoothed by randomizing around a ± 10 Ma range to reduce spikes in estimated ages. Where no measured age is available for a geochemistry sample, the age is estimated from the geological unit it was taken from. Note that vertical height has not significance for magma volumes. b. Igneous bedrock U–Pb age spectra of 248 individual zircons from 9 samples collected from the Peruvian Coastal Batholith near Ica, adapted from Martínez et al. (2019).

Across-strike petrological changes have also been described for the south and central segments. The high Pb-isotope ratios indicate that subducted sediments were incorporated into the mantle sources (Couch et al., 1981; Martínez Ardila et al., 2019a, 2019b and Mukasa, 1986). Martínez Ardila et al. (2019a, 2019b) suggested that the across-arc chemical variation in the Ica-Pisco plutons of the central segment resulted from three magma sources consisting of the mantle reservoir, subducted sediments, and old continental crust, with different degrees of contamination by subducted sediments at the mantle source and crustal assimilation during magma transport and emplacement. These geochemical variations from older western to younger eastern plutons show an initial decrease in the mantle component, a general increase in the isotopically evolved component, and an initial increase and later decrease in the volcanic and plutonic host rock components.

4.2.1. Synthesis of geochemical data

Our geochemical dataset (see the Supplementary Data) comes from integrating new with published data. The INGEMMET database that

became available in 2021 (<http://metadatos.ingemmet.gob.pe:8080/geonetwork/srv/eng/catalog.search#/home>) is complemented with the most recent dataset published by Martínez Ardila et al. (2019a, 2019b), plus new geochemical data. We present new whole-rock geochemical data of major and trace elements from >1000 samples, and Sr, Nd, and Pb isotope ratios from 87 samples of the PCB (see the Supplementary Data) in Figs. 4–8. New whole rock samples were analyzed for major element chemistry at the ALS laboratories using a Thermo Jarrell Ash Enviro II simultaneous and sequential ICP with a detection limit from 0.001 to 0.01% for major elements, from 0.002 to 0.05 ppm for REE, and from 0.01 to 20 ppm for other trace elements. Two instrumentation techniques were used by ALS Laboratories to obtain the chemical data: ICM90A using sodium peroxide fusion analyzed via ICP-MS for trace elements, and ICP95A using lithium metaborate fusion analyzed via ICP atomic emission spectroscopy (AES) for major and some trace elements. The isotopic ratios of $^{87}\text{Sr}/^{86}\text{Sr}$ and $^{143}\text{Nd}/^{144}\text{Nd}$ and the trace element concentrations of Rb, Sr, Sm, and Nd were measured by thermal ionization mass spectrometry in the

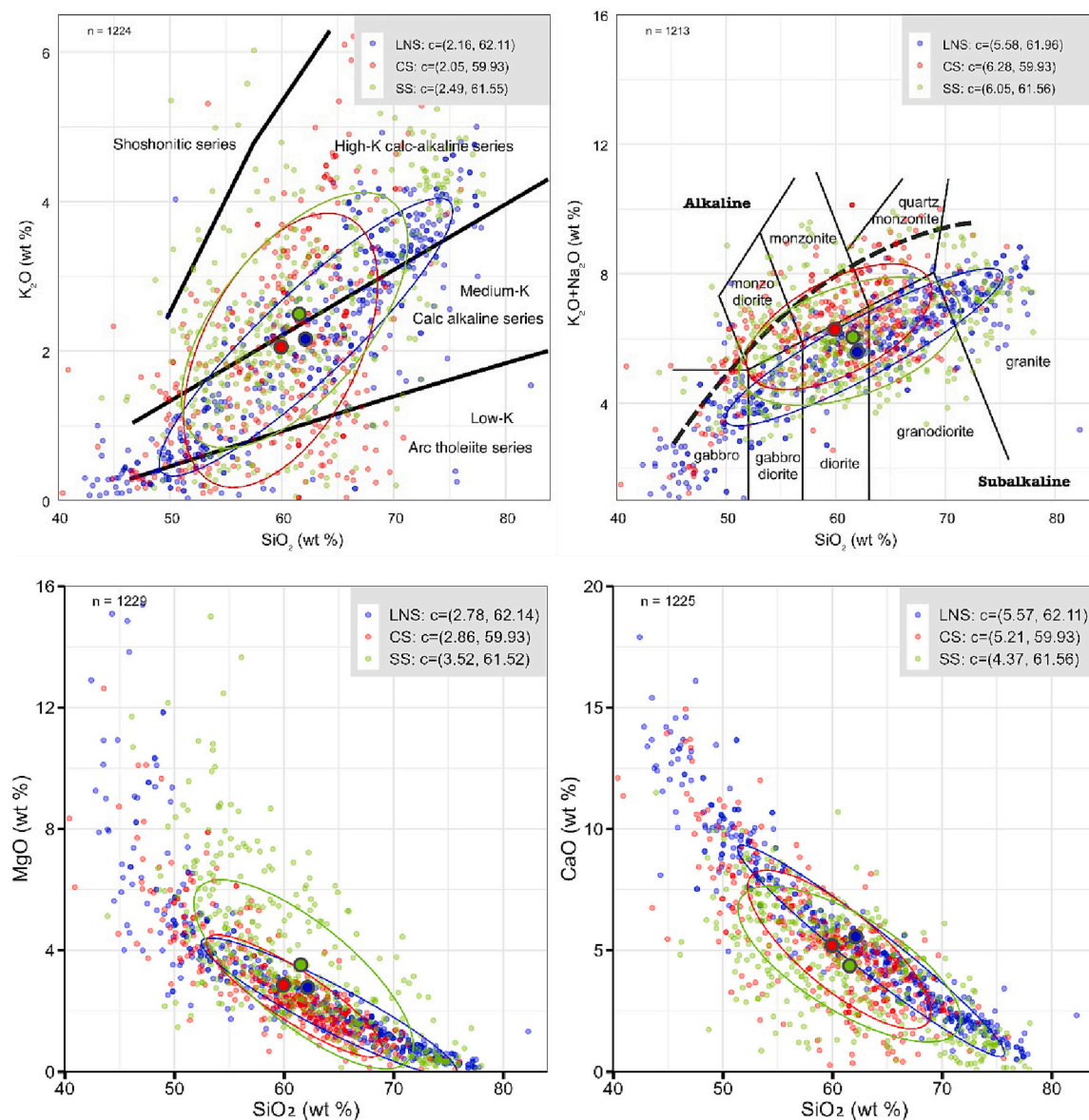


Fig. 4. Harker diagrams of selected major oxides for the PCB segments using our suggested boundaries: South Segment (SS), Central Transitional Segment (CS), and Lower Northern Segment (LNS). Datasets includes plutonic and associated volcanic rocks. Statistical analyses were run on the compiled datasets to calculate the mean for identifying trends and evaluate the boundaries for each segment (Supplementary Data 1). The ovals are used in the plots to emphasize the different trends of the plutons.

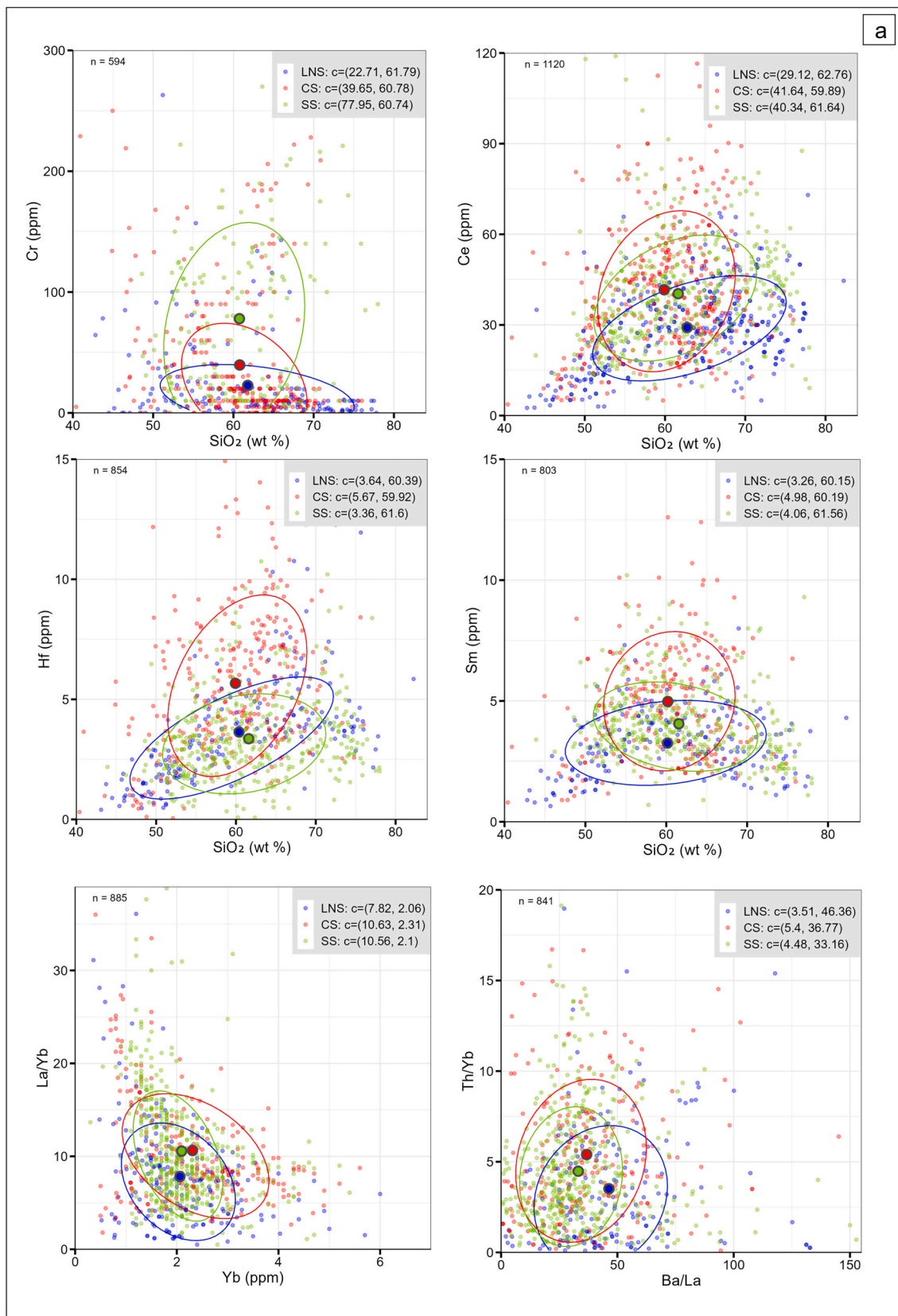


Fig. 5. (a) Along-arc Harker diagrams trace elements for the PCB using our suggested boundaries: South Segment (SS), Central Transitional Segment (CS), and Lower Northern Segment (LNS). Statistical analyses were run on the compiled datasets to calculate the mean for identifying trends and evaluate the boundaries for each segment (Supplementary Data). (b) Along-arc REE multi-elemental. Primitive mantle (P-mantle) normalization data are from Sun and McDonough (1989).

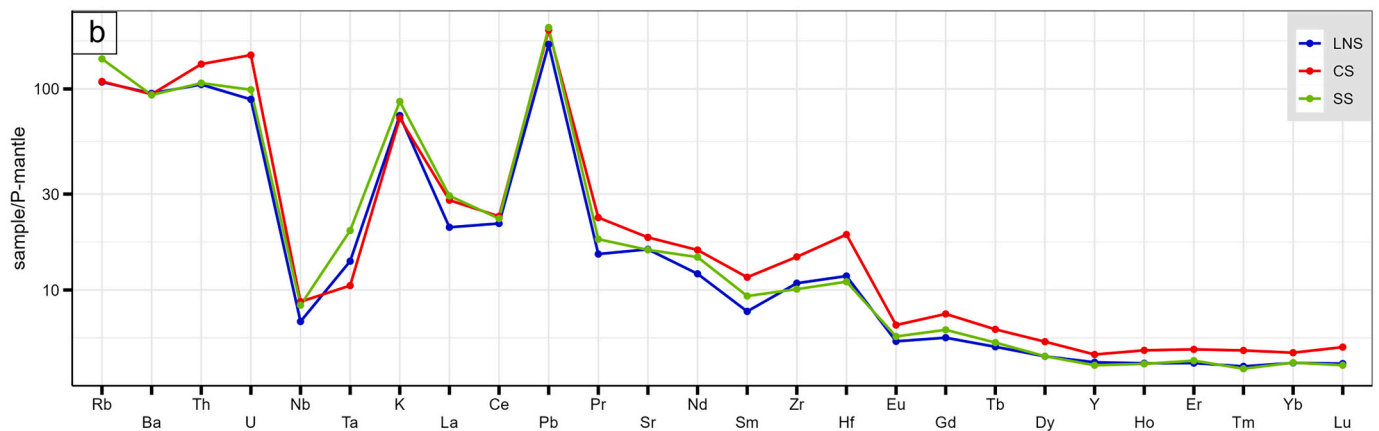


Fig. 5. (continued).

Geochronology and Thermochronology Lab of the University of Arizona and were performed on a VG Sector TIMS instrument using the techniques described by Ducea (1998) and Otamendi et al. (2009). The common isotopes of lead were analyzed on separate batches of dissolved samples. Lead was extracted using an anion exchange procedure modified after Chen and Wasserburg (1981).

We use quartz $\delta^{18}\text{O}$ values to estimate the primary oxygen isotopic composition in our analysis. Oxygen isotopes were analyzed using the laser fluorination method of Sharp (1990) and a ThermoFinnigan DeltaPlus XP mass spectrometer at IIRMES, California State University, Long Beach. Quartz is the major rock forming mineral in intermediate to felsic igneous rocks that is most resistant to subsolidus isotopic exchange as the result of hydrothermal processes (Gregory et al., 1989). The 65 samples chosen for this study contain rock-forming mineral assemblages that meet the criteria of $^{18}\text{O}/^{16}\text{O}$ equilibrium using the method of Javoy et al. (1970).

4.3. Spatial and temporal variations

Previous investigations focused on the geochemical trends of the Lima and Arequipa segments (Fig. 1). For this reason, less information is available for the Piura, Trujillo, and Toquepala segments, so this limits our ability to compare all the PCB segments and requires a different approach to synthesize the PCB data.

Statistical analyses were run on the compiled datasets to calculate the mean for identifying trends and evaluate the boundaries for each segment. Limited age and chemical data for the upper northern PCB (4–8°S) makes it difficult to identify temporal and chemical trends and is not included in this study. Our suggested along-arc segments are lower northern (LNS at 8–12.5°S), central transitional (CS at 12.5–15°S), and southern (SS at 15–18.4°S), and across arc zones are west-to-east distance. For these divisions of the PCB, we will study different flare-ups based on U–Pb zircon ages (200–20 Ma). The suggested new boundaries are based on the mean of chemical proxies and abrupt changes in the distribution of samples. In a first approach, Fig. 3a displays the geochronological data used to define the flare-ups and Figs. 4 to 8 display the chemical data using our suggested boundaries.

Figs. 4 through 8 summarize the variation of geochemical parameters along- and across-arc in the PCB. The PCB chemical signature is predominantly metaluminous with calc-alkaline affinities. The chemical differences along-arc segments are recognized by changes in the following proxies: K_2O , CaO , MgO , Cr , Ce , Hf , Sm , and La/Yb elements, and Sr_i , $\delta^{18}\text{O}$, and Pb isotopes. The chemical changes can be grouped in two categories: (1) elements that decrease from the SS to the LNS, K_2O (2.5 to 2.13 wt%), MgO (3.51 to 2.78 wt%), Ce (40.42 to 29.12 ppm), La/Yb (10.58 to 7.84), Sr_i (0.758 to 0.704), and $\delta^{18}\text{O}$ (8.85 to 8.38); and (2) elements that increase from the SS to the LNS, CaO (4.36 to 5.57 wt

%), and ϵNd (–0.87 to 2.53). The changes identified reveal that the SS is significantly different from the LNS. In addition, we conclude that the CS between 12.5°S and 15°S is a transitional boundary between the LNS and SS, because it exhibits gradual changes for most of the chemical proxy values. The CS is distinguished by having the highest values of Hf (5.64 ppm), Sm (4.98 ppm), Th/Yb (5.39), and $^{207}\text{Pb}/^{204}\text{Pb}$ and $^{206}\text{Pb}/^{204}\text{Pb}$ isotopes (15.64 and 18.68 respectively) in the PCB. In general, from S to N there is a decrease of K_2O , MgO , Cr , Ce , La/Yb , Sr_i , and $\delta^{18}\text{O}$ and an increase of CaO and ϵNd (Table 1).

Quartz $\delta^{18}\text{O}$ values from the northern segment range from +7.1‰ to +9.7‰ ($n = 24$), with an average of 8.38‰ (Fig. 6b). These values are consistent with whole rock $\delta^{18}\text{O}$ values (between +5.7‰ and +7.6‰, $n = 11$) reported by Beckinsale et al. (1985) from the 65 Ma Cañas/Sayan plutonic complex at Rio Hualar in the LNS. The CS exhibits slightly higher average quartz $\delta^{18}\text{O}$ values (+8.68‰, this study and Gonzalez et al., 2020) than the LNS with a range of +7.3‰ to +9.7‰ ($n = 24$). SS rocks have a bimodal distribution of oxygen isotope values that are age dependent (Fig. 9). Plutons older than 120 Ma have quartz $\delta^{18}\text{O}$ values that average +10.0‰ ($n = 8$) and a range of +8.4‰ to +12.0‰. In contrast, plutons younger than 120 Ma have lower and more homogeneous quartz $\delta^{18}\text{O}$ values (+7.7‰ to +8.5‰, $n = 9$) that average +8.1‰.

The across-arc, west-east trends of the PCB were defined using perpendicular distance of samples from the Andean foothills. The western zone is <30 km from the beginning of foothills; the central zone is between 30 and 60 km; and the eastern zone is >60 km. Again, the chemical changes can be grouped in two categories: (1) elements and isotopes that decrease from W to E, CaO (5.85 to 4.3 wt%), MgO (3.83 to 2.53 wt%), Cr (48.05 to 41.04 ppm), ϵNd (1.55 to 0.61), and $^{206}\text{Pb}/^{204}\text{Pb}$ (18.68 to 18.37); and (2) elements and isotopes that increase from W to E, K_2O (1.78 to 2.69 wt%), Ce (33 to 46.6 ppm), Hf (4.18 to 4.51 ppm), Sm (4.09 to 4.45 ppm), La/Yb (7.89 to 12.51), Th/Yb (3.56 to 5.06), $\delta^{18}\text{O}$ (8.46 to 8.99), Sr_i (0.7047 to 0.7057). The central zone exhibits gradual changes for most of the chemical proxies, but lower values of MgO (2.16 wt%), Cr (33.58 ppm), and Hf (3.81 ppm). A general trend from W to E is the decrease in CaO , MgO , ϵNd , and $^{206}\text{Pb}/^{204}\text{Pb}$, and an increase of K_2O , Ce , Hf , La/Yb , Sr_i , and $\delta^{18}\text{O}$ (Table 2).

Primitive mantle-normalized multielement patterns along- and across-arc segments of the PCB (Fig. 5b and 8d) observe strong negative anomalies for Nb and positive for K and Pb, enrichment in large-ion lithophile elements (LILEs), light rare earth elements (LREE), and depletion in heavy rare earth elements (HREE). Slightly LILE enriched patterns are observed for the SS and CS with respect to the LNS. These segments show an enrichment of LILEs (e.g., Rb, K, Sr, Pb, Eu) and high-field strength elements (HFSEs) (e.g., La, Th, U, Hf, Nb) compared to the LNS. Across-arc trends for the C and E zones are slightly more enriched in large-ion lithophile elements (LILEs) (e.g., Rb, Ba, Th, K), but more

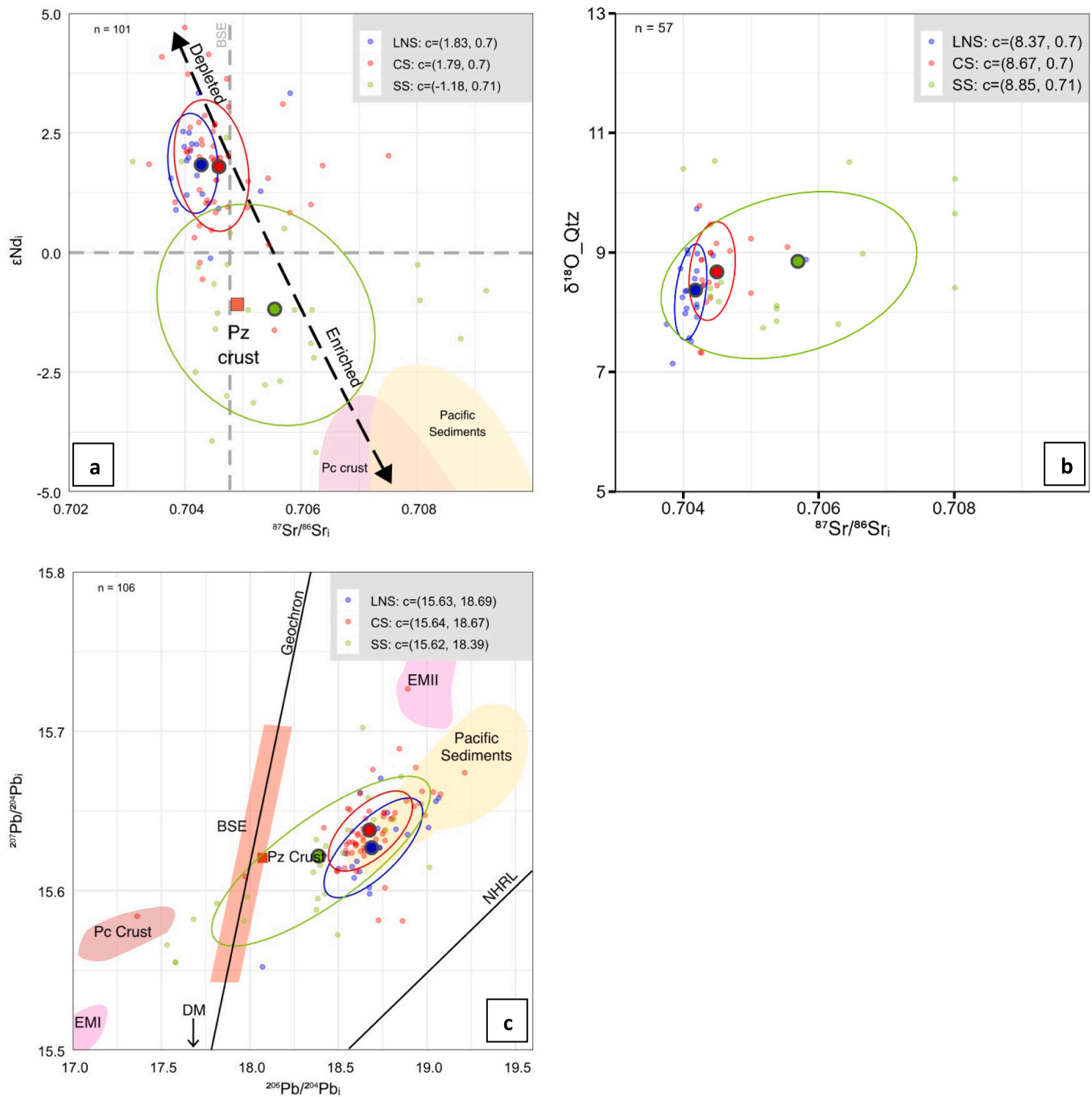


Fig. 6. Isotopes (a) Isotope ratios of Nd and Sr. The data show a slight increase of Sr_i towards younger and more evolved plutons. Paleozoic (Pz) and Precambrian (Pc). (b) $\delta^{18}\text{O}$ for quartz. Note the slight increasing trend from LNS towards the CTS and SS. (c) Magma sources and variation of $^{207}\text{Pb}/^{204}\text{Pb}_i$ versus $^{206}\text{Pb}/^{204}\text{Pb}_i$. For comparison, five fields are included: depleted mantle (DM), Pacific sediments and Precambrian and Paleozoic crust. The line labeled NHRL (Northern Hemisphere Regression line) denotes the approximate lower limit of mid-ocean ridge basalt (MORB) Pb isotopic signatures. Pacific Sediment data is from Reynolds and Dasch (1971) and Chow and Patterson (1962); Precambrian crust data from Mukasa (1986); mantle reservoir data from Zindler and Hart (1986), and our data.

depleted in heavy rare earth elements (HREE) (e.g., Ho, Er, Tm, Yb) than the W zone.

4.3.1. Age spectra for the PCB

The measured bedrock U–Pb crystallization ages from mafic and felsic compositions for the PCB yield the flare-ups depicted in Fig. 3a for ages between 200 and 20 Ma for the three segments (Supplementary Data). Four flare-ups were identified in the PCB lower north segment (LNS-1, LNS-2, LNS-3, LNS-4), three in the central transitional segment (CS-1, CS-2, CS-3) and four in the south segment (SS-1, SS-2, SS-3, SS-4).

Our results reveal a general trend of northward and eastward younging ages. The spatiotemporal trend shows magmatism migrating from S to N, with an early Jurassic flare-up (~200–174 Ma) identified in the SS and a late Paleogene flare-up (~52–22 Ma) identified in the LNS. This study reveals along-arc variation during periods of increased magmatic activity, where flare-ups are temporally offset between neighboring segments. Older flare-ups started first in the SS. This S to N trend represents a W to E migration of the magmatic arc as well (Table 3).

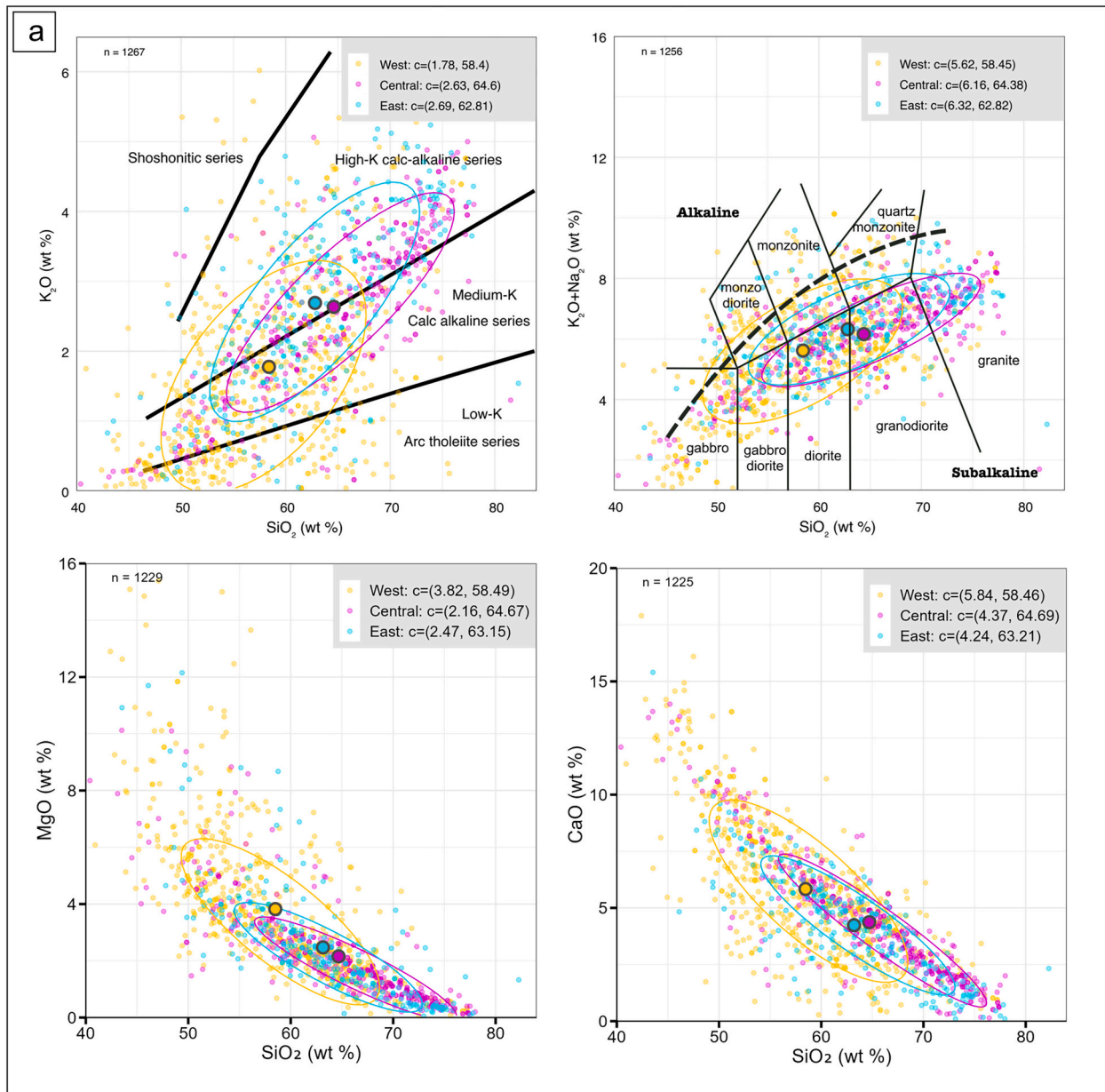


Fig. 7. a. Harker diagrams of selected trace elements for the PCB across-arc segments using our suggested boundaries: West, Central, and East. Datasets include plutonic and associated volcanic rocks. Statistical analyses were run on the compiled datasets to calculate the mean for identifying trends (Supplementary Data 1). b. Harker diagrams of selected trace elements for the PCB across arc segments using our suggested boundaries: West, Central, and East. Datasets include plutonic and associated volcanic rocks. Statistical analyses were run on the compiled datasets to calculate the mean for identifying trends (Supplementary Data 1).

4.3.2. West to east arc migration for Plutons near Pisco

U—Pb zircon ages for the PCB shown in Fig. 1 show that arc magmatism migrated from west to east. Specifically, we have studied this west to east migration in the Pisco area.

U—Pb zircon ages published by Martínez Ardila et al. (2019a, 2019b) displayed the W to E migration of the magmatic arc in the CS of the PCB. Fig. 3b displays U—Pb zircon ages plotted as the 248 individual zircons that make up 9 igneous bedrock samples averaging about 25 zircons each. The order of crystallization for major units of the Ica-Pisco plutons started in the W with gabbro-diorite plutons in the Early Cretaceous (131.0 Ma), followed by Linga Auquish (104.8 Ma), Linga Rinconada (98.3 Ma), Pampahuasi (97.8 and 91.4 Ma), Tiabaya (85.3 and 84.4 Ma) and finally in the E with Incahuasi (68 and 58 Ma) in the

Early Paleogene.

4.4. Moho depth calculations for crustal thickness

Present-day crustal thickness for the Central Andes decreases from 60 to 65 km in the SS and CS at about 8–12°S to 40–45 km in the LNS at about 12–7°S (James, 1971; Schmitz, 1994; Dorbath, 1996; Swenson et al., 2000). Present-day crustal thickness increases from west to east in the LNS and CS from ~20 km up to 45 km, and in the SS from 40 km up to 60 km (Schellart, 2017). Crustal thickness is hard to estimate for past geological times; however, it appears that the Central Andean crust underwent significant thinning up until 90 Ma (Sempere et al., 2002), slowly started thickening after 90 Ma, and experienced a significant

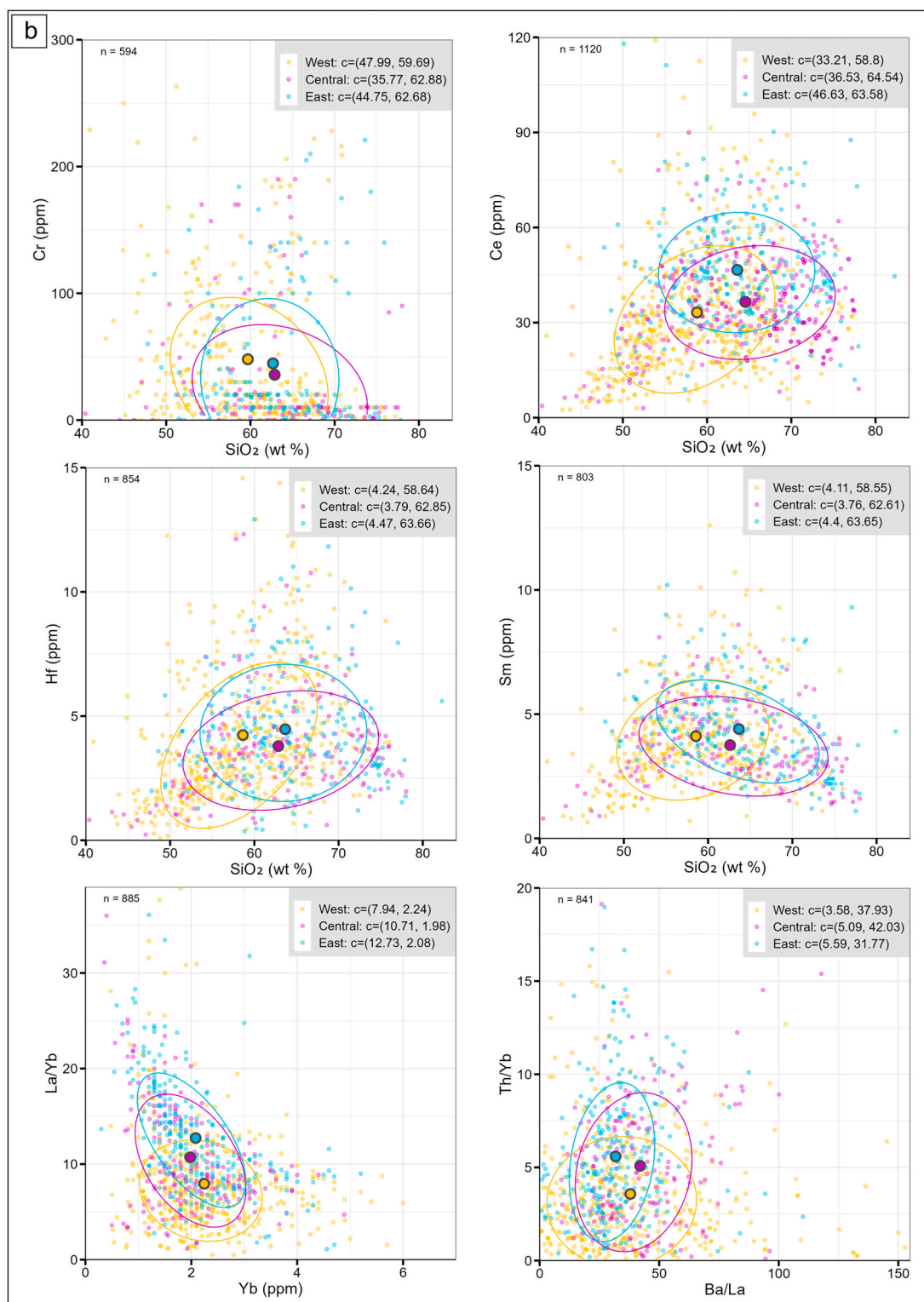


Fig. 7. (continued).

thickening after 30 Ma in association with tectonic shortening (e.g., Ganne et al., 2017; Garziona et al., 2008; Gregory-Wodzicki, 2000; Isacks, 1988; Mamani et al., 2010).

To qualitatively determine changes in crustal thickness from the Jurassic (~200 Ma) to Pleistocene (~1 Ma) in the Central Andes, Mamani et al. (2010) identified changes in Dy/Yb and Sm/Yb ratios. Lavas younger than 30 Ma have high Dy/Yb and Sm/Yb ratios; rocks older than 30 Ma display lower $^{87}\text{Sr}/^{86}\text{Sr}$, Dy/Yb, and Sm/Yb ratios; and

rocks older than 91 Ma have even lower $^{87}\text{Sr}/^{86}\text{Sr}$, Dy/Yb, and Sm/Yb ratios. This suggests that major crustal thickening began in the mid-Oligocene at about 30 Ma and that crustal thickness has continued to increase until the present.

To estimate crustal thickness for the three segments of the PCB (Supplementary Data), Moho depth estimates were obtained from multiple whole rock chemical proxies following the method outlined by Luffi and Ducea (2022) and using age bins defined by major episodic

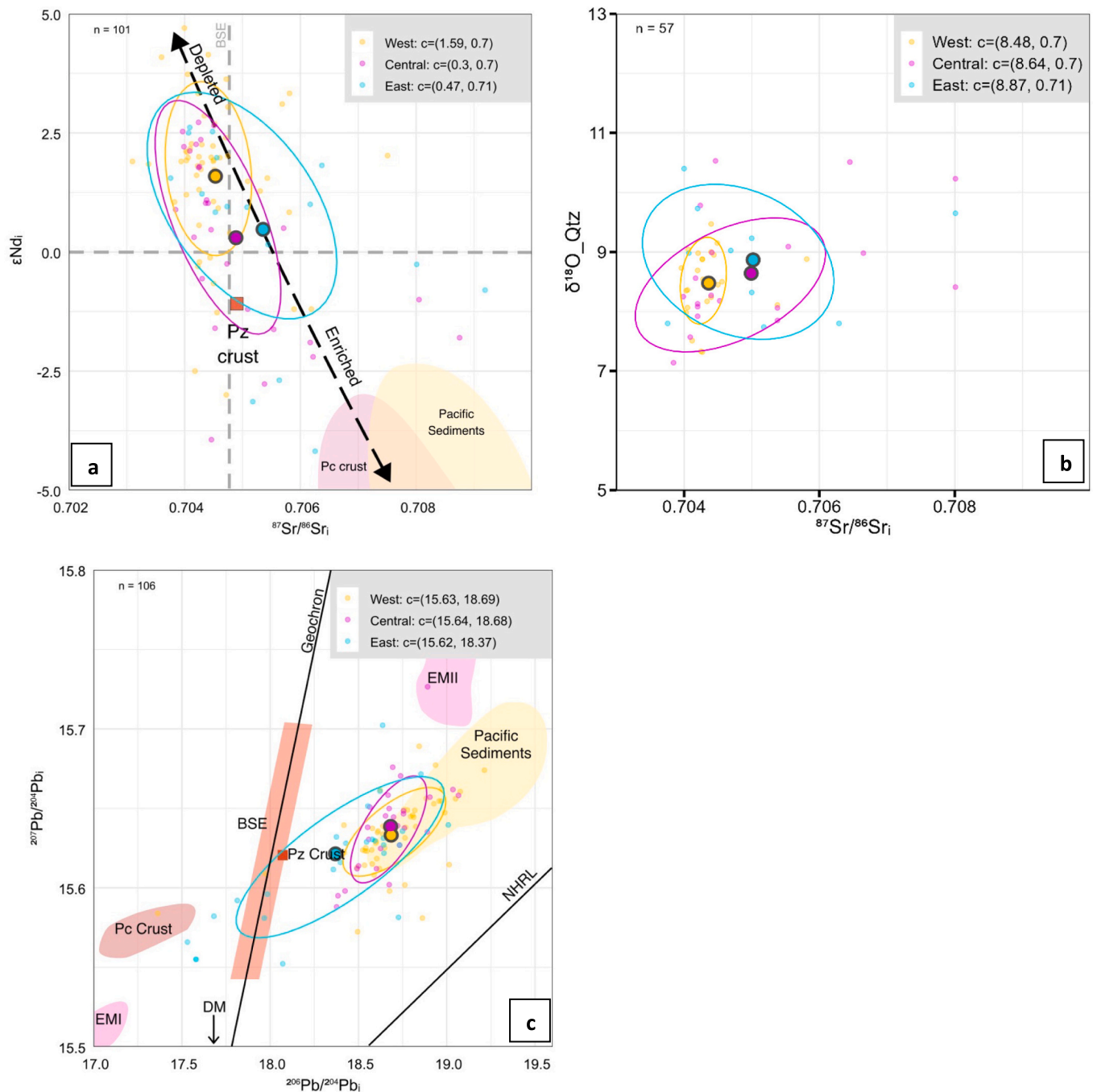


Fig. 8. Isotopes (a) Isotope ratios of Nd and Sr. The data show a slight increase of Sr_i towards younger and more evolved plutons. Paleozoic (Pz) and Precambrian (Pc). (b) $\delta^{18}\text{O}$ for quartz. Note the slight increasing trend from LNS towards the CTS and SS. (c) Magma sources and variation of $^{207}\text{Pb}/^{204}\text{Pb}_i$ versus $^{206}\text{Pb}/^{204}\text{Pb}_i$. For comparison, five fields are included: depleted mantle (DM), Pacific sediments and Precambrian and Paleozoic crust. The line labeled NHRL (Northern Hemisphere Regression line) denotes the approximate lower limit of mid-ocean ridge basalt (MORB) Pb isotopic signatures. Pacific Sediment data is from Reynolds and Dasch (1971) and Chow and Patterson (1962); Precambrian crust data from Mukasa (1986); mantle reservoir data from Zindler and Hart (1986), and our data. (d) Across-arc REE multielemental. Primitive mantle (P-mantle) normalization data are from Sun and McDonough (1989).

flare-ups of magmatism for each segment (see Fig. 3). Our approach has limitations because the geochronological and geochemical data do not have a one-to-one correspondence, i.e., each geochemical data set does not necessarily have an associated U–Pb age. Thus, the geochemistry used for the Moho calculations for each flare-up are not exactly the same flare-ups defined by our geochronological dataset. Recognizing this limitation, our calculations have estimated crustal thickness evolution from south to north as follows: (1) the Southern PCB thickens from 34

km at ~ 200 Ma to 43 km at ~ 89 Ma and then thins to 39 km at ~ 60 Ma; (2) the Central PCB has less dramatic changes, starting with constant thickness at 36 km at ~ 139 –73 Ma and then thickening to 43 km at ~ 60 Ma; (3) the lower Northern PCB shows a constant thickness of 29 km at ~ 116 –87 Ma and then thickening from 34.5 km at ~ 84 Ma to 42.5 km at ~ 22 Ma. In summary, crust for the LNS and CS was thinner in the middle Cretaceous and thickened during the late Cretaceous and into the early Cenozoic (Fig. 9). The SS was different because a thinning episode

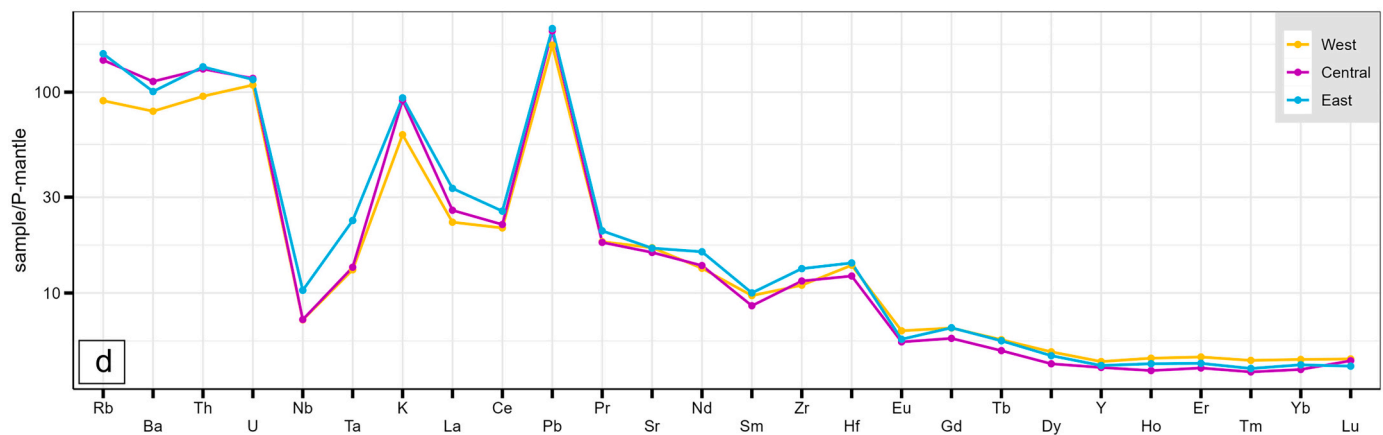


Fig. 8. (continued).

Table 1
Chemical trends along-arc segments.

Chemical Proxy	Trend from S to N
K ₂ O, MgO, Ce, Cr, La/Yb, Sr _i , δ ¹⁸ O	SS > CS > LNS
CaO, εNd	SS < CS < LNS
Hf, Sm, Th/Yb, and Pb isotopes	Low-High-Low

started in the late-Cretaceous and continued until the late-Eocene (~85–38 Ma).

4.5. Assimilation and fractional crystallization (AFC)

Elemental and isotopic variation in igneous rocks can be modeled using crustal contamination or assimilation and fractional crystallization (AFC) calculations (DePaolo, 1981). Previous AFC modeling of the PCB includes the work by Boily et al. (1989) on the SS and Martínez Ardila et al. (2019a, 2019b) on the CS. Boily et al. (1989) proposed an AFC model requiring first a lower Precambrian crust and then a middle upper Precambrian crust to explain the geochemical diversity of the plutonic rocks. Martínez Ardila et al. (2019a, 2019b) suggested that magmas in the central transitional segment are made up of 70% mantle, 20% subducted oceanic sediments, and assimilation of 10% lower crust (Precambrian and Paleozoic) and upper crust (Mesozoic volcanic and plutonic units).

To address the causes of the geochemical variation along the PCB, we did AFC modeling of the potential crustal contributions for each of the arc segments using Sr elemental and isotopic compositions (Fig. 10). The first step is selection of the input parameters for the end members and the bulk partition coefficient (D). The end members for each segment are the parental mantle melt composition (C₀) and the potential assimilants (C_a): Pacific sediments, Precambrian and Paleozoic basement, and altered oceanic crust (AOC). The most primitive sample in the dataset are used to approximate C₀ (e.g., Keskin, 2013; Stracke et al., 2003). For C_a, three values were considered to estimate a likely maximum amount of crust assimilated: (1) the respective composition of the crustal basement in each segment from our geochemical dataset, (2) chemical and isotope data of Pacific sediments from Chow and Patterson (1962) and Reynolds and Dasch (1971), and (3) values for AOC from Ishikawa and Tera (1999). The Sr bulk partition coefficient (D) used in the modeling is from Rollinson (1993) and the GERM Kd database for basalts (<https://earthref.org/GERM/>).

The modeled curves used different values of r which is the ratio of mass assimilation rate to fractional crystallization rate. The input parameters determine the position and shape of the modeled curves, so the parameters are varied for the three datasets until a reasonable fit to the data occurs (Fig. 10). The most representative AFC fits for the Sr data for

each segment are explained below.

South Segment: Parental mantle magmas assimilated up to ~20–25% of Precambrian crust during fractional crystallization at the emplacement level. Possibly minor contamination from Paleozoic crust and Pacific sediments in the source region could also take place. In Fig. 10a it is observed that the assimilation is lower during the 118–89 Ma episode and increases with the younger 85–38 Ma flare-up.

Central Transitional Segment: In CS parental mantle magmas interacted with three types of assimilants: (1) Pacific sediments with ~5–10% assimilation in the source region, (2) basement with ~10–15% assimilation of altered oceanic crust, and (3) minor Precambrian and Paleozoic crustal assimilation during fractional crystallization. The assimilation of isotopically evolved materials increased through time reaching a maximum at 70–50 Ma (Fig. 10b).

Lower North Segment: The model curves for the LNS indicated that contamination of parental magmas in this segment resulted from a less evolved end member characterized by low Sr and Sr_i values (Fig. 10c). This suggests that the ~20–30% assimilation observed in the LNS is derived from AOC and took place during fractional crystallization. Our AFC modeling cannot identify assimilation of continental crust or Pacific sediments observed in the other segments or changes in the amount of assimilation through time.

5. Discussion

5.1. Modern overview of the PCB

Construction of the PCB began in the Early Jurassic when a magmatic arc developed along the western margin of Gondwana in an attenuated crust within an extensional tectonic setting that changed to strongly contractional in the Late Cretaceous (Jaillard and Soler, 1996; Matthews et al., 2012; Pardo-Casas and Molnar, 1987; Ramos, 2018; Soler and Bonhomme, 1990).

Plutons were emplaced through two different basements. The SS arc magmas were emplaced in older ~1900 Ma continental crust of the Arequipa terrane and the CS and LNS magmas in the younger ~1200 Ma continental crust of the Paracas terrane where an intra-arc Cretaceous basin developed by attenuation of preexisting crust (Ramos and Alemán, 2000). The boundary between the CS and SS coincides with the suture zone between the Arequipa and Paracas terrains. Therefore, there is a strong link between the chemical changes along-arc in the PCB and the type of basement where the plutons are emplaced (Dalmayrac et al., 1977; Mamani et al., 2010).

The geochemical and geochronological data presented in this study display along-strike and across-strike variations in basement types and/or crustal thickness, magma sources, magmatic differentiation processes, and amounts of crustal assimilation through time and space for

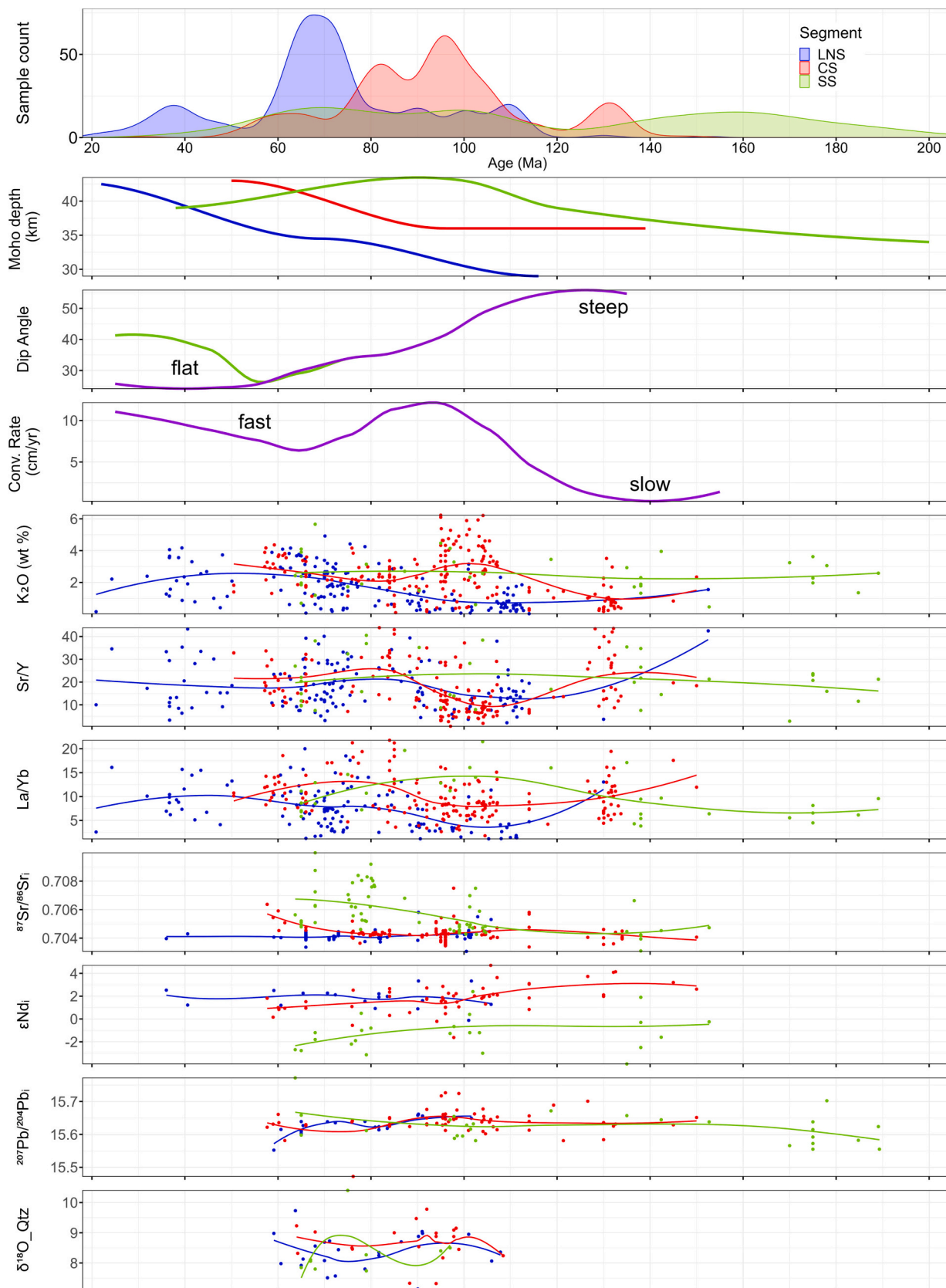


Fig. 9. Age histogram and whole-rock petrogenetic indicators. The geochemical data are used to estimate crustal thickness. All geochemical parameters are plotted according to the outcrop age. Data source includes our new age and chemical data and compiled whole rock data (Supplementary Data): South Segment (SS), Central Transitional Segment (CS), and Lower Northern Segment (LNS).

Table 2
Chemical trends across-arc segments.

Chemical Proxy	Trend from W to E
K ₂ O, Ce, Hf, Sm, La/Yb, Th/Yb, Sr _i	W < C < E
Ca, MgO, εNd, ²⁰⁶ Pb/ ²⁰⁴ Pb	W > C > E
Cr	High-Low-High
²⁰⁷ Pb/ ²⁰⁴ Pb	Low-High-Low

Table 3
summarizes the parameters for each flare-up, including the range, duration, peak and Moho depth.

Flare-up	Range (Ma)	Duration (Ma)	Peak (Ma)	Moho Depth (Km)
SS-1	200–174	26	182	34
SS-2	170–131	39	162	39
SS-3	118–89	29	98	43
SS-4	85–38	47	66	39
CS-1	139–124	15	131	36
CS-2	117–73	44	96	36
CS-3	70–50	20	64	43
LNS-1	116–101	15	109	29
LNS-2	97–87	10	91	29
LNS-3	84–54	30	70	34.5
LNS-4	52–22	30	37	42.5

the PCB. Uranium-lead zircon age patterns for the PCB display along-arc variation in the timing of increased magmatic activity, where the oldest flare-up started in the southern segment and flare-ups progressing north are temporally offset (not continuous) between neighboring segments. We defined 4 flare-ups for the SS from ~200 to 38 Ma, 3 flare-ups for the CS from ~139 to 50 Ma, and 3 flare-ups for the LNS from ~116 to 22 Ma.

We will discuss possible causes for the spatial and temporal chemical trends in the PCB segments by integrating: (1) patterns of episodic magmatism and linked chemical data, (2) tectonic setting and subduction parameters that characterized magmatic episodes, (3) calculations of Moho depths, and (4) estimates of mantle and crustal contributions through time and space.

South Segment: In the SS the magmatic arc was emplaced in the Arequipa terrane where the tectonic setting changed from extension in the Jurassic to contraction in the Cretaceous to extension again in the Paleogene. Four magmatic episodes are defined at 200–174 Ma, 170–131 Ma, 118–89 Ma, and 85–38 Ma. The first three flare-ups started with a continental crust of ~34 km that thickened to 43 km by the end of the 118–89 Ma flare-up, possibly associated with the emplacement of plutons and the beginning of a contractional regime. The arc in this segment records high values for K₂O, La/Yb, and Sr_i (Fig. 4). These values indicate a magma source consisting of ~70% mantle affected by ~25–30% continental crustal contamination from the old Arequipa Precambrian and Paleozoic basement rocks (Fig. 10b).

Central Transitional Segment: In this CS the magmatic arc was emplaced in the northern end of the Arequipa terrane and the southern end of the Paracas terrane. The transition lies near the Abancay-Andahuaylas shear zone (SZAA), a structure that has been suggested as the boundary between the two terranes (Ccallo Morocco et al., 2021; Mamani et al., 2010; Ramos, 2018). This is supported by the observed gradual chemical changes across this structure. Three magmatic episodes are observed at 134–124 Ma, 117–73 Ma, and 70–50 Ma. The first two flare-ups occurred primarily during extension with minimal change in crustal thickness. The final 70–50 Ma magmatic episode occurred at the beginning of a contractional regime as the continental crust thickened from ~36 km to 43 km. The high values of Ce, Hf, and Sm plus the REE whole rock geochemistry indicate more fractionated magmas. The La/Yb ratio is similar to that for the SS rocks and might indicate a deep magma source, suggesting a greater possibility for assimilation during magma ascent. Sr and Nd isotopes are primitive and indicate a

significant contribution from mantle melting (Fig. 9 and 10c). Whereas Pb isotopes suggest assimilation of 15–20% oceanic crust combined with melting/fluids from 5 to 10% subducted Pacific Ocean sediments and minor assimilation from Precambrian and Paleozoic basement during magma ascent and emplacement. Geochemical variations from older to younger plutons show a decrease in the mantle component.

Lower North Segment: In the LNS the magmatic arc was emplaced in the Paracas terrane. Four magmatic episodes are observed at 116–101 Ma, 97–87 Ma, 84–54 Ma, and 54–22 Ma. The first two flare-ups occurred in thin ~29 km crust during a continuous contractional setting, high convergence rates, and therefore coupling between plates. The crust eventually thickened to 42 km by the end of the 52–22 Ma flare-up. The arc in this segment records low values for K₂O, La/Yb, Sr_i, and Pb isotopes. These values indicate magmas coming from a shallower magma source and the contamination of ~70% mantle magmas by ~20–30% assimilation of altered oceanic crust with minor involvement of continental crust. In the LNS the chemical proxies show various spatiotemporal patterns seemingly unrelated to assumed changes in the subduction parameters and tectonic settings throughout the magmatic episodes.

5.1.1. Across-arc petrological variations

The values of K₂O (1.78 to 2.69 wt%), Ce (33 to 46.6 ppm), Hf (4.18 to 4.51 ppm), La/Yb (7.89 to 12.51), Sr_i (0.7047 to 0.7057), and δ¹⁸O (8.46 to 8.99) increase towards the east suggesting a more evolved signature of the arc there (Figs. 7 and 8). The La/Yb ratio and REE whole rock geochemistry indicate that the youngest inboard plutons have a deeper magma source, suggesting a thicker lower crust with greater possibility for assimilation during magma ascent. The arc migrated to the east through time during which magma chemistries experienced an increase in K₂O, La/Yb ratio, δ¹⁸O, Sr_i, and Pb isotopes. An increase in assimilation as the arc migrates to the east can be predicted by crustal thickening, but this may not be the only explanation for the observed petrological variations. Instead, these isotopically evolved signatures can be linked to partial melting of the mantle that occurs farther away from the trench in response to slab flattening and may reflect incorporation of continental lithospheric mantle in the melt region (Chapman et al., 2017).

5.2. Causes of compositional diversity

5.2.1. Flare-ups, magma sources, and assimilation

The along-arc trend in the PCB from south to north is towards less evolved Sr, Nd, and Pb isotopes. This can be explained by a combination of four factors: (1) interaction of arc magmas with two different basement types, i.e., the Arequipa continental crust or the Paracas attenuated continental crust covered by mafic pillow lavas and pyroclastic rocks interfingering with marine sediments (Mamani et al., 2008; Ramos, 2010; Ramos, 2018), (2) variation of crustal assimilation at emplacement levels associated with changes in crustal thickness (Cobbing and Pitcher, 1972), (3) a changing amount of subducted sediment assimilated at the magma source, and (4) the nature of the mantle reservoir (Martínez Ardila et al., 2019a, 2019b; Mukasa, 1986).

The geochemical evidence suggests that granitoids in the SS of the PCB have been modified by magmas rising through the Arequipa terrane assimilating Precambrian and Paleozoic basement (Beckinsale et al., 1985; Boily et al., 1989). More limited crustal contamination was previously suggested for the CS and LNS, but this is questionable. The primitive composition associated with the Paracas terrane means that a less evolved crustal isotope signature could have still been assimilated in significant amounts. The high Pb isotope ratios observed especially in the CS supports the interpretation that both basement and subducted Pacific sediments were assimilated into the mantle magmas that formed the plutons of the CS (Couch et al., 1981; Martínez Ardila et al., 2019a, 2019b; Mukasa, 1986).

Quartz δ¹⁸O values of +7.1‰ to +12.0‰ cover the entire range of

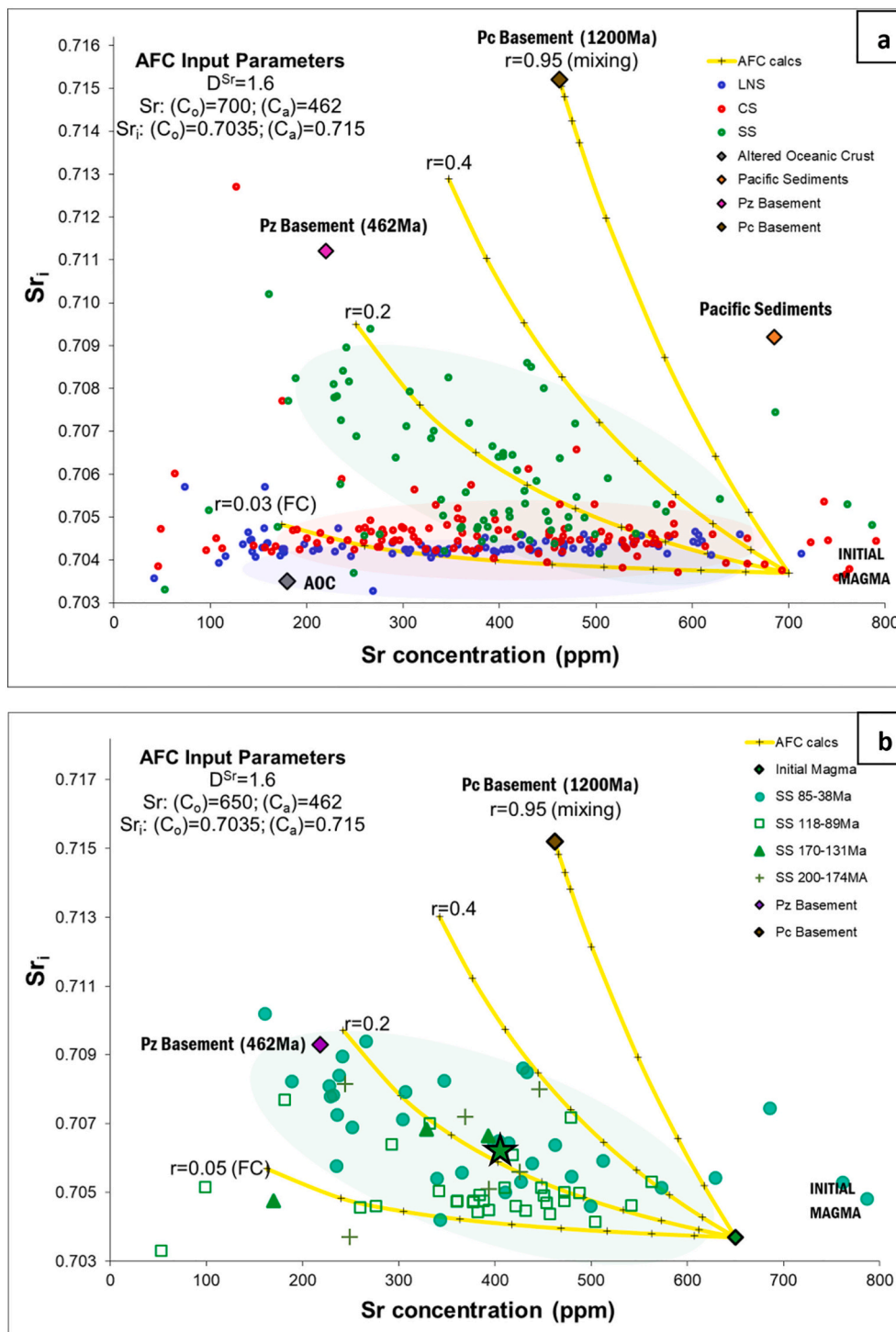


Fig. 10. AFC modeling for Sr_1 vs. Sr plot. The initial magma composition uses a Sr_1 and Sr values suggested for parental mantle (Gale et al., 2003; Faure, 2009). Color fields represent the distribution of the samples, and the star symbol indicates their respective averages. (a) Higher assimilation of Pc crust in the SS. The maximum amounts of crust assimilated to form the arcs are: (b) 25% Pc with minor Pz crust for the SS; (c) 10–15% for AOC (Altered Oceanic Crust) and 10% Pacific sediments for CS, and (c) an average of 30% AOC for LNS.

values produced by variable mixtures of (1) melt derived from the mantle where quartz $\delta^{18}O \sim +7\%$; (e.g., Eiler, 2001; Zheng, 1993) and (2) melts of material that experienced at least one cycle of surficial weathering (e.g., Taylor Jr. and Sheppard, 1986) or low temperature alteration on the seafloor (e.g., Hanson et al., 1993; Holk et al., 2008) resulting in quartz $\delta^{18}O$ values $> +12.0\%$. This ambiguity can be resolved by using a radiogenic isotope tracer such as Sr in conjunction

with $\delta^{18}O$ values (e.g., James, 1982; Kistler et al., 2014; Lackey et al., 2008), which can distinguish between older and younger assimilants and whether assimilation is due to source or crustal contamination. Our data clearly indicate crustal contamination (Fig. 6b), as $\delta^{18}O$ values rise at a greater rate than $^{87}Sr/^{86}Sr_1$ values. Most plutons lie on a trend between a depleted mantle primary magma source with low $\delta^{18}O$ and $^{87}Sr/^{86}Sr_1$ and a young weathered/altered assimilant with high $\delta^{18}O$ and

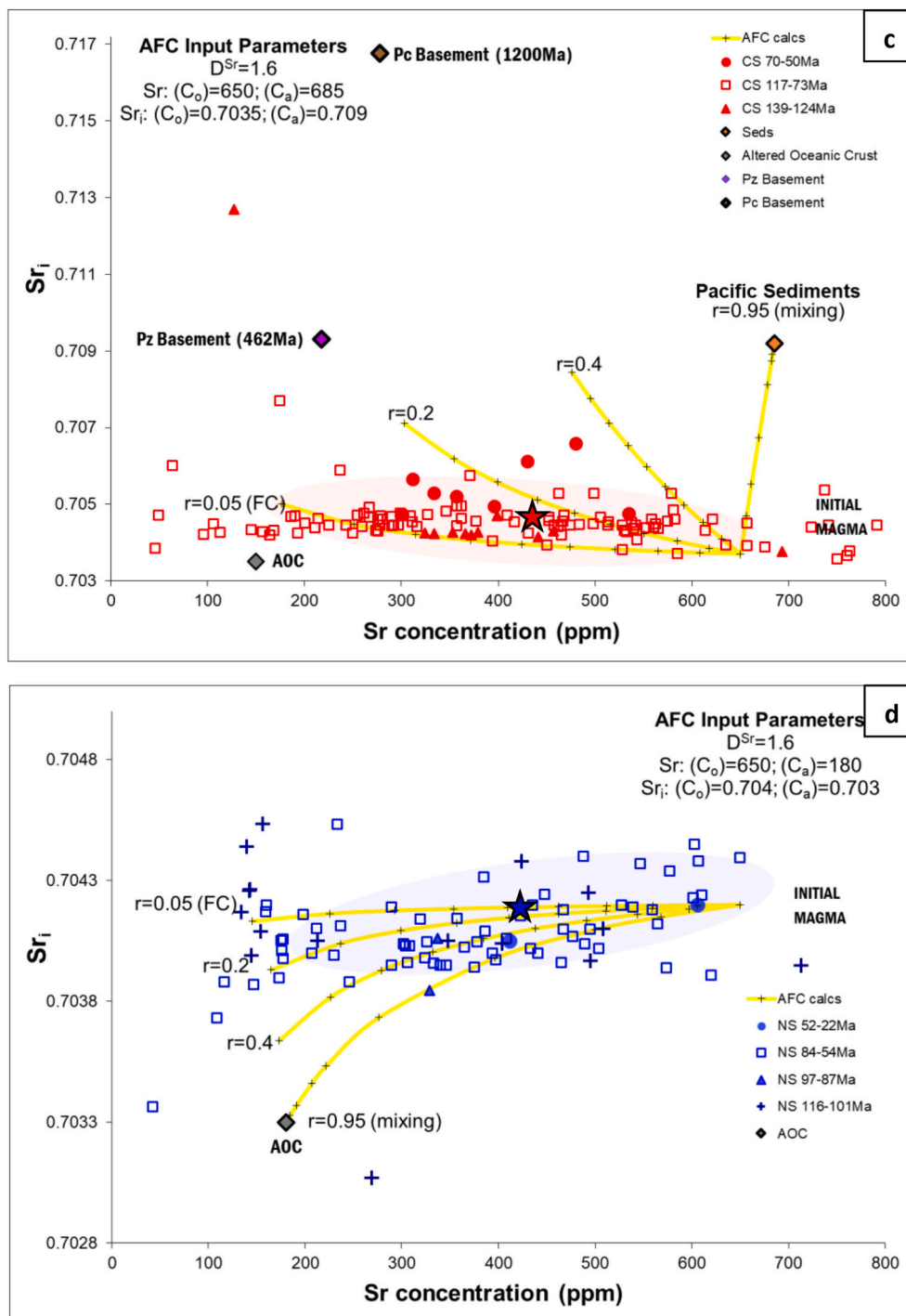


Fig. 10. (continued).

low initial $^{87}Sr/^{86}Sr$, consistent with altered oceanic crust or volcanoclastic sediments deposited in the Huarmey-Canete Basin. The exceptions are the >120 Ma plutons from the SS and a few plutons from the CS, which display variable $\delta^{18}O$ values and more evolved $^{87}Sr/^{86}Sr_i$ values indicating the incorporation of an older assimilant, such as Precambrian basement rocks of the Arequipa Terrane.

The Sr, Nd, and Pb isotopes and $\delta^{18}O$, as well as AFC modeling, indicate that the relative contributions from mantle and crust differ for different arc segments. They also show that the PCB magmas have experienced fractional crystallization with <20–30% crustal assimilation, implying that the great majority of these magmas are mantle-

derived. Thus, since the greatest volumetric change during flare-ups is an increase in mantle magmas, the flare-ups must result largely from episodic mantle processes; crustal melting was not required for triggering the flare-up and only played a secondary role in modifying melt compositions.

5.2.2. Crustal thickness

Previous studies of Central Andean magmatism have concluded that the thickened crust has strongly affected Andean arc magmas through crustal contamination (e.g., DeCelles et al., 2009; Kay et al., 1994, 1999; Kay et al., 1999; Wörner et al., 2000). The same has been assumed for

the PCB, i.e., the composition of the PCB was strongly affected by magmas intruded into and traversing a thick continental crust (Beckinsale et al., 1985; Boily et al., 1989). If correct, an increase in Sr/Y, La/Yb, and Sr_i is explained as the result of crustal thickening and linked with arc magma production (Haederle and Atherton, 2002; Mamani et al., 2010). However, the compositional changes identified in the PCB are not expected to be the same through time because the thickness of the crust has changed as well (see Table 3 and Fig. 9).

Magma addition to the arc displays a non-steady-state pattern of temporal and spatial scales, and available estimates of magma addition are insufficient to explain all of the observed crustal thickness changes (Trumbull et al., 2006; Wörner et al., 2000). Besides crustal thickness, alternative mechanisms to change chemical compositions have been proposed, such as “source contamination” by subduction erosion of the forearc (Clift and Hartley, 2007; Kay et al., 2005; Stern et al., 1981), or the influence of enriched subcontinental mantle lithosphere in the source region (Rogers and Hawkesworth, 1989). If partial melting occurs further away from the trench as the arc migrates, it can incorporate higher amounts of lithospheric mantle and the resulting magmas will show a more evolved chemical signature (Chapman et al., 2021). In that case, these chemical changes may reflect not only changes in crustal thickness but also lateral migration of the arc resulting in magma passing through crust with different chemical properties and an increase in lithospheric mantle input (Kirsch et al., 2016; Paterson et al., 2016).

5.2.3. The role of tectonism

In the past, links between tectonic processes and magma compositions have been suggested for the PCB (Mamani et al., 2010). Five aspects of tectonics can be considered when evaluating such relationships between tectonics and magmatism in arcs: (1) motions of subducting plates, (2) tectonic styles in arcs, (3) crustal thicknesses. (4) relations between individual plutons and regional deformation (e.g., faults, folding), and (5) tectonic triggers for magma flare-ups. We have not presented the appropriate data to discuss #4 and will not discuss this aspect further.

An examination of Fig. 9 shows no correlations between subduction parameters and arc flare-ups or geochemistry in the PCB, a result that is typical for arcs elsewhere (Chapman et al., 2021; Kirsch et al., 2016; Paterson and Ducea, 2015).

Tectonic regimes in the PCB have clearly changed through time from a dominantly regional extensional regime from Early Jurassic to Early Cretaceous (190–120 Ma) to a contractional regime in Late Cretaceous during which large sections of the forearc were removed by subduction erosion (120 to 80 Ma) and significant mountain building began (80–70 Ma). In spite of these widespread changes, data in Fig. 9 indicate that different arc segments responded to these shifting tectonic regimes in different ways including crustal thicknesses and arc geochemistry. In general, our spatiotemporal reconstructions in Fig. 9 reveal no clear (consistent) coupling between PCB segments nor between tectonic regimes and magma geochemistry. Instead our dataset reinforces the idea of complexity in the arc requiring interactions between multiple causes to yield the final arc signatures.

Triggers of arc flare-ups have been a topic of much recent interest in the geologic community (DeCelles et al., 2009; Kirsch et al., 2016; Martínez Ardila et al., 2019a, 2019b; Paterson and Ducea, 2015). In previous studies including our own, attempts to determine triggers for magmatic flare-ups largely focused on determining if they were external (lower plate) or internal (upper plate) with the latter also being divided between potential crustal or mantle processes. We now recognize that a complex interplay likely occurs between all of these, with external processes controlling fairly instantaneous boundary conditions for arc behavior, while upper plate processes are influenced by long composite histories of continental margins. In other words, the characteristics of the mantle and overlying crustal columns, upon which the external boundary conditions are superposed, has evolved over 10s to 100 s of millions of years. As noted in many other studies of flare-ups in arcs

(Chapman et al., 2021; Kirsch et al., 2016; Martínez Ardila et al., 2019a, 2019b), we see no correlations between external plate motion features and flare-ups (Fig. 9). But this is likely because the signal of changing boundary conditions is filtered in complex ways by responses of a very heterogeneous mantle/crustal arc column.

In the PCB the spatial and temporal variability of arc flare-ups, mantle and basement types, tectonic regimes, crustal thicknesses and igneous geochemistry imply that an equivalent temporal-spatial variability is needed for flare-up triggers. For example, not every flare-up is associated with thick crust and lulls are not necessarily associated with thin crust. And geochemical data do not show consistent patterns during flare-up initiations, nor in flare-ups in different arc segments. To us, this suggested “variability of triggers” implies a variability in how different processes interacted. Even so, much of our geochemical data and modeling point towards the importance of mantle sources to produce the greatest volume of magmatism during flare-ups suggesting that episodic mantle processes likely play the dominate role in triggering flare-ups.

Episodic mantle processes (both external and internal) are thus a ripe target for future studies of arc flare-up triggers. For example, plate motion (such as convergence rate) might influence the behavior of the mantle (England and Katz, 2010; Turner and Langmuir, 2015). Higher convergence rates can produce more hydration of the mantle wedge (e.g., Cagnioncle et al., 2007; Plank et al., 2009), and/or increase the temperature of the mantle wedge corner (England and Katz, 2010; England and Wilkins, 2004; Turner and Langmuir, 2015) resulting in an increase in mantle melting.

5.2.4. Missing datasets: ages to define flare-ups and spatial and temporal trends

In order to correlate magma composition with the evolution of crust for the PCB, the sequence of magmatic events and associated geochemical signatures must be constrained by absolute ages. In the past, timing of magmatism in the PCB was somewhat poorly understood due to heavy dependence on whole-rock Rb—Sr and K—Ar geochronology, both of which can yield questionable crystallization ages due to low closure temperatures and isotopic disturbances by subsequent thermal episodes (Dodson, 1973). This is a particularly acute problem in Peru where ~150 m.y. of uninterrupted subduction occurs during the Andean orogenic cycle (Benavides Cáceres, 1999). More ages and chemical data are still needed for the upper northern segment, since we were not able to fully characterize it: our restricted dataset for this segment allowed us to only examine the most southern part of the northern section.

Timing of PCB emplacement also needs to consider whether the Jurassic magmatism is due to back-arc volcanism or a different subduction-related process and why it is volumetrically restricted.

Finally, we recognize that the ideas presented in this paper should be re-evaluated as larger and more precise geochronological, geochemical, and plate kinematic data sets become available in the future.

6. Conclusions

This paper presented a complete compilation and analysis of all available geochronological, geochemical, and plate kinematic datasets for the PCB, including our new data, to clarify the temporal and spatial record of magmatic events and provide a more rigorous interpretation of the causes of arc magmatism and its chemical diversity. Below, we summarize five major contributions of our work.

- (1) The magmatic episodes in the PCB are now better characterized using zircon geochronology coupled with whole-rock geochemical analyses. The PCB shows a clear non-steady-state pattern of magmatism at variable temporal and spatial scales, including between arc segments (Fig. 1 and 3). Some flare-ups are discrete, but others are synchronous for hundreds of kilometers along-arc and exhibit a periodicity of 30–40 m.y. We find no evidence to

support a continuous and volumetrically constant pattern of magmatism in the PCB, as previously used to support the “superunit” concept.

- (2) Arc magma chemistry varies in both space and time, including between arc segments (Figs. 4–7 and 9). The identified chemical diversity both along- and across-arc are the result of changing upper plate mantle input (transitioning from depleted to lithospheric mantle), types of upper plate basement (i.e., Paracas and Arequipa terranes), varying types and degrees of assimilated material from Pacific sediments, changing crustal thickness, arc migration, and the extent of magma fractionation.
- (3) We find no convincing correlations between arc chemistry and plate motion phenomena such as convergence rate and dip angle. However, upper plate tectonic phenomena, such as styles of tectonics (extension, contraction, transpression) and/or crustal thickness may show weak relationships to geochemical signals, although it is typically hard to fully separate different tectonic effects from other parameters such as mantle and basement type.
- (4) In previous studies, including our own, attempts to determine triggers for magmatic flare-ups largely focused on determining if they were external (lower plate) or internal (upper plate) with the latter also being divided into crustal or mantle processes. We now recognize that a complex interplay likely occurs between all of these with external processes controlling fairly instantaneous boundary conditions for arc behavior while upper plate processes are influenced by lengthy composite histories of continental margins. Even so we see no correlations between plate motion features and flare-ups (Fig. 9). The spatial and temporal variability of arc flare-ups, mantle and basement types, tectonic regimes, crustal thicknesses and igneous geochemistry in the PCB signals an equivalent variability in flare-up triggers. However much of our geochemical data and modeling point towards the importance of mantle sources to produce the greatest volume of magmatism indicating that episodic mantle processes likely play the dominant role in triggering flare-ups.
- (5) Possibly the most important result is the documentation of the incredible heterogeneity of both tectonic and magmatic arc behavior over short spatial lengths. Therefore, the causes also have to be heterogeneous over these length scales. Most data presented in Fig. 9 points to both along and across arc complexity, including from one segment to the next and from one flare-up to the next. This complexity must reflect a dynamic interaction between lower plate driven boundary conditions on upper plate long term evolution of mantle, crustal basement and evolving magma systems.

Declaration of Competing Interest

The authors declare that they have no known competing financial interests or personal relationships that could have appeared to influence the work reported in this paper.

Acknowledgements

The authors acknowledge financial support for this study from Loma Linda University and the Geoscience Research Institute (Projects GRI2014-BC01 and GRI2015-AM10). We thank Orlando Poma for his valuable assistance during fieldwork. We thank the lab scientists at the Arizona LaserChron Center for help while using their geochronology lab. We are especially grateful to the Bendezu Family for their kindness and hospitality during our visits to Peru. We also would like to thank the editor Greg Shellnutt and reviewers Victor Ramos and Francisco Pereira for their useful comments that helped improve the quality of the manuscript. Martínez-Ardila thanks Felipe Pichinual for data synthesis and drafting help, Luiz Pereira and Alex Voos for helping with data compilation.

Appendix A. Supplementary data

Supplementary data to this article can be found online at <https://doi.org/10.1016/j.lithos.2023.107298>.

References

- Agar, R., 1978. The Peruvian Coastal Batholith: Its Monzonitic Rocks and their Related Mineralization. The Geology of the Rio Pisco, a Sector of the Arequipa Segment of the Coastal Batholith [Doctor of Philosophy. University of Liverpool (293 p)].
- Arndt, N.T., Goldstein, S.L., 1989. An open boundary between lower continental crust and mantle: its role in crust formation and crustal recycling. *Tectonophysics* 161 (3–4), 201–212.
- Aspden, J.A., McCourt, W.J., Brook, M., 1987. Geometrical control of subduction-related magmatism: the Mesozoic and Cenozoic plutonic history of Western Colombia. *J. Geol. Soc.* 144 (6), 893–905.
- Atherton, M., Aguirre, 1992. Thermal and geotectonic setting of cretaceous volcanic rocks near Ica, Peru, in relation to Andean crustal thinning. *J. S. Am. Earth Sci.* 5 (1), 47–69.
- Atherton, M., Pitcher, W., Warden, V., 1983. The Mesozoic marginal basin of Central Peru. *Nature* 305 (5932), 303–306.
- Atherton, M., Warden, V., Sanderson, L., 1985. The Mesozoic marginal basin of Central Peru: A geochemical study of within-plate-edge volcanism. In: Pitcher, W.S., et al. (Eds.), *Magmatism at a Plate Edge: The Peruvian Andes*. John Wiley, New York, pp. 47–58.
- Attia, S., Cottle, J.M., Paterson, S.R., 2020. Erupted zircon record of continental crust formation during mantle driven arc flare-ups. *Geology* 48 (5), 446–451.
- Bahlburg, H., Carlotto, V., Cárdenas, J., 2006. Evidence of early to Middle Ordovician arc volcanism in the Cordillera oriental and Altiplano of southern Peru, Ollantaytambo Formation Umachiri beds. *J. S. Am. Earth Sci.* 22 (1–2), 52–65.
- Beck, S.L., Zandt, G., 2002. The nature of orogenic crust in the Central Andes: Journal of Geophysical Research: Solid Earth 107 (B10) (p. ESE 7-1-ESE 7-16).
- Beckinsale, R.D., Sanchez-Fernandez, A.W., Brook, M., Cobbing, E.J., Taylor, W.P., Moore, N.D., 1985. Rb-Sr whole-rock isochrons and K-Ar age determinations for the Coastal Batholith of Peru. In: Pitcher, W.S., et al. (Eds.), *Magmatism at a Plate Edge: The Peruvian Andes*. John Wiley, New York, pp. 177–202.
- Bellido Bravo, E., 1969. Sinopsis de la Geología del Perú. *Boletín Servicio Geológico Minero del Perú* 22, 54.
- Bellido, F., Valverde, P., Jaimes, F., Carlotto, V., Díaz-Martínez, E., 2009. Datación y caracterización geoquímica de los granitoides peraluminicos de los cerros de Amotape y de los Macizos de Illescas y Paita (Noroeste de Perú). *Boletín Sociedad Geológica del Perú* 103, 197–213.
- Benavides Cáceres, V., 1999. Orogenic evolution of the Peruvian Andes: the Andean cycle. In: Skinner, B. (Ed.), *Geology and mineral deposits of Central Andes*, 7. Society of Economic Geology Special Publication, pp. 61–107.
- Boily, M., Brooks, C., Ludden, J.N., 1989. Chemical and isotopic evolution of the Coastal Batholith of southern Peru. *J. Geophys. Res.* 94 (89), 12483–12489.
- Bussell, M.A., Pitcher, W.S., 1985. The structural controls of batholith emplacement. In: Pitcher, W.S., et al. (Eds.), *Magmatism at a Plate Edge: The Peruvian Andes*. John Wiley, New York, pp. 167–176.
- Bussell, M.A., Pitcher, W.S., Wilson, P.A., 1976. Ring complexes of the Peruvian Coastal Batholith: a long-standing subvolcanic regime. *Can. J. Earth Sci.* 13 (8), 1020–1030.
- Cagnioncle, A.M., Parmentier, E., Elkins-Tanton, L.T., 2007. Effect of solid flow above a subducting slab on water distribution and melting at convergent plate boundaries. *J. Geophys. Res. Solid Earth* 112 (B09402). <https://doi.org/10.1029/2007JB004934>.
- Cao, W., Paterson, S., Saleeby, J., Zalunardo, S., 2016. Bulk arc strain, crustal thickening, magma emplacement, and mass balances in the Mesozoic Sierra Nevada arc. *J. Struct. Geol.* 84, 14–30.
- Cardona, A., Cordani, U.G., Nutran, A., Zimmermann, U., Sanchez, A.W., 2005. Tectonic setting and geochronology of Pre-Llanvirian metamorphic rocks of the Marañón Complex (E. Peru): from rifting to collision to form the Rheic ocean: Gondwana 12 “geological and biological, heritage of Gondwana”.
- Carlotto, V., Quispe, J., Acosta, H., Rodríguez, R., Romero, D., Cerpa, L., Mamani, M., Díaz-Martínez, E., Navarro, P., Jaimes, F., 2009. Dominios geotectónicos y metalogénesis del Perú. *Boletín de la Sociedad Geológica del Perú* 103 (1), 1–89.
- Casquet, C., Fanning, C.M., Galindo, C., Pankhurst, R.J., Rapela, C.W., Torres, P., 2010. The Arequipa Massif of Peru: New SHRIMP and isotope constraints on a Paleoproterozoic inlier in the Grenvillian orogen. *J. S. Am. Earth Sci.* 29 (1), 128–142.
- Castro, A., Rodríguez, C., Fernández, C., Aragón, E., Pereira, M.F., Molina, J.F., 2021. Secular variations of magma source compositions in the North Patagonian batholith from the Jurassic to Tertiary: was mélange melting involved? *Geosphere* 17 (3), 766–785.
- Castro, A., Vogt, K., Gerya, T., 2013. Generation of new continental crust by sublithospheric silicic-magma reamination in arcs: a test of Taylor’s andesite model. *Gondwana Res.* 23 (4), 1554–1566.
- Castroviejo Bolibar, R., Rodrigues, J.F., Carrascal, R., Chirif, H., Acosta, J., Uribe, R., 2009. Mineralogía del Macizo Ultramáfico de Tapo (Cordillera Oriental Andina, Perú): Revista de la Sociedad Española de Mineralogía, Macla, 11, pp. 55–56.
- Cealio Morocco, W.E., López Aguilar, Y.P., Guo, W., Liu, J., Chen, S., Duan, Z., 2021. Características litogeoquímicas y petrográficas en los bordes norte y sur del segmento Lima-Batolito de la Costa, comparada con el sureste de China. *Instituto Geológico Minero y Metalúrgico del Perú “INGEMMET” D (35)*, 10–12.

- Chapman, J., Ducea, M., Kapp, P., Gehrels, G., DeCelles, P., 2017. Spatial and temporal radiogenic isotopic trends of magmatism in Cordilleran orogens. *Gondwana Res.* 48, 189–204.
- Chapman, J.B., Shields, J.E., Ducea, M.N., Paterson, S.R., Attia, S., Ardill, K.E., 2021. The causes of continental arc flare ups and drivers of episodic magmatic activity in Cordilleran orogenic systems. *Lithos* 398. <https://doi.org/10.1016/j.lithos.2021.106307>.
- Chen, J.H., Wasserburg, G.J., 1981. Isotopic determination of uranium in picomole and subpicomole quantities. *Anal. Chem.* 53 (13), 2060–2067.
- Chin, E.J., Lee, C.-T.A., Blichert-Toft, J., 2015. Growth of upper plate lithosphere controls tempo of arc magmatism: Constraints from Al-diffusion kinetics and coupled Lu-Hf and Sm-Nd chronology. *Geochem. Perspect. Lett.* 1, 20–32.
- Chow, T.J., Patterson, C., 1962. The occurrence and significance of lead isotopes in pelagic sediments. *Geochim. Cosmochim. Acta* 26 (2), 263–308.
- Clark, A.H., Farrar, E., Kontak, D.J., Langridge, R.J., Arenas, F., France, L.J., McBride, S. L., Woodman, P.L., Wasteneys, H.A., Sandeman, H.A., 1990. Geologic and geochronologic constraints on the metallogenic evolution of the Andes of southeastern Peru. *Econ. Geol.* 85 (7), 1520–1583.
- Clift, P.D., Hartley, A.J., 2007. Slow rates of subduction erosion and coastal underplating along the Andean margin of Chile and Peru. *Geology* 35 (6), 503–506.
- Cobbing, E., 1978. The Andean geosyncline in Peru, and its distinction from Alpine geosynclines. *J. Geol. Soc.* 135 (2), 207–218.
- Cobbing, E.J., 1985. The Central Andes: Peru and Bolivia: the Ocean Basins and margins: volume 7A. *Pacific Ocean* 219–264.
- Cobbing, E.J., Ozard, J.M., Snelling, N.J., 1977. Reconnaissance geochronology of the crystalline basement rocks of the Coastal Cordillera of southern Peru. *Geol. Soc. Am. Bull.* 88 (2), 241–246.
- Cobbing, E.J., Pitcher, W.S., 1972. The Coastal Batholith of Central Peru. *J. Geol. Soc.* 128 (5), 421–454.
- Cobbing, E.J., Pitcher, W.S., 1983. Andean plutonism in Peru and its relationship to volcanism and metallogenesis at a segmented plate edge. *Geol. Soc. Am. Mem.* 159, 277–291.
- Couch, R., Whiltsett, R.M., Huehn, B., Briceno-Guarupe, L., 1981. Structures of the continental margin of Peru and Chile. In: Kulm, L.D., Dymond, J., Dasch, E.J., Hussong, D.M., Geological Society of America Memoirs (Eds.), *Nazca Plate: Crustal Formation and Andean Convergence*, 154, pp. 703–726.
- Dalmayrac, B., Lancelot, J., Leyreloup, A., 1977. Two-billion-year granulites in the late Precambrian metamorphic basement along the southern Peruvian coast. *Science* 198 (4312), 49–51.
- Daly, M.C., 1989. Correlations between Nazca/Farallon plate kinematics and forearc basin evolution in Ecuador. *Tectonics* 8 (4), 769–790.
- De Haller, A., Corfú, F., Fontboté, L., Schaltegger, U., Barra, F., Chiaradia, M., Frank, M., Alvarado, J.Z., 2006. Geology, geochronology, and Hf and Pb isotope data of the Raúl-Condestable iron oxide-copper-gold deposit, central coast of Peru. *Econ. Geol.* 101 (2), 281–310.
- DePaolo, D.J., 1981. Trace element and isotopic effects of combined wallrock assimilation and fractional crystallization. *Earth Planet. Sci. Lett.* 53 (2), 189–202.
- de Silva, S.L., Riggs, N.R., Barth, A.P., 2015. Quickening the Pulse: Fractal Tempos in Continental Arc Magmatism. *Elements* 11 (2), 113–118.
- de Silva, S.L., Gosnold, W.D., 2007. Episodic construction of batholiths: Insights from the spatiotemporal development of an ignimbrite flare-up. *J. Volcanol. Geotherm. Res.* 167 (1–4), 320–335.
- DeCelles, P.G., Ducea, M.N., Kapp, P., Zandt, G., 2009. Cyclicity in Cordilleran orogenic systems. *Nat. Geosci.* 2 (4), 251–257.
- DeCelles, P.G., Zandt, G., Beck, S.L., Currie, C.A., Ducea, M.N., Kapp, P., Gehrels, G.E., Carrapa, B., Quade, J., Schoenbohm, L.M., 2015. Cyclical Orogenic Processes in the Cenozoic central Andes, 212. Geological Society of America Memoirs, pp. 459–490.
- Díaz-Martínez, E., Acosta, H., Cárdenas, J., Carlotto, V., Rodríguez, R., 2001. Paleozoic diamicites in the Peruvian Altiplano: evidence and tectonic implications. *J. S. Am. Earth Sci.* 14, 587–592.
- Dodson, M.H., 1973. Closure temperature in cooling geochronological and petrological systems. *Contrib. Mineral. Petrol.* 40 (3), 259–274.
- Dorbath, C., 1996. Velocity structure of the Andes of Central Peru from locally recorded earthquakes. *Geophys. Res. Lett.* 23 (2), 205–208.
- Ducea, M., 1998. A Petrologic Investigation of Deep-Crustal and Upper-Mantle Xenoliths from the Sierra Nevada, California: Constraints on Lithospheric Composition beneath Continental Arcs and the Origin of Cordilleran Batholiths [PhD Dissertation]. California Institute of Technology (364 p).
- Ducea, M.N., 2001. The California arc: Thick granitic batholiths, eclogitic residues, lithospheric-scale thrusting, and magmatic flare-ups. *GSA Today* 11, 4–10.
- Dunbar, R.B., Marty, R.C., Baker, P.A., 1990. Cenozoic marine sedimentation in the Secura and Pisco basins, Peru. *Palaeogeogr. Palaeoclimatol. Palaeoecol.* 77 (3–4), 235–261.
- Eiler, J.M., 2001. Oxygen isotope variations of basaltic lavas and upper mantle rocks. *Rev. Mineral. Geochem.* 43 (1), 319–364.
- Ellison, R., Klinck, B., Hawkins, M., 1989. Deformation events in the Andean orogenic cycle in the Altiplano and Western Cordillera, southern Peru. *J. S. Am. Earth Sci.* 2 (3), 263–276.
- England, P.C., Katz, R.F., 2010. Melting above the anhydrous solidus controls the location of volcanic arcs. *Nature* 467 (7316), 700–703.
- England, P., Wilkins, C., 2004. A simple analytical approximation to the temperature structure in subduction zones. *Geophys. J. Int.* 159 (3), 1138–1154.
- Espurt, N., Funicello, F., Martinod, J., Guillaume, B., Regard, V., Faccenna, C., Brusset, S., 2008. Flat subduction dynamics and deformation of the south American plate: Insights from analog modeling. *Tectonics* 27 (3). <https://doi.org/10.1029/2007TC002175>.
- Fanlo, I., Gervilla, F., Castroviejo, R., Rodrigues, J.F., Pereira, E., Acosta, J., Uribe, R., 2009. Metamorphism of chromitites in the Tapo ultramafic massif, Eastern Cordillera, Peru. In: *Proceedings 10th Biennial SGA Meeting, Townsville, Australia*, pp. 161–163.
- Feininger, T., 1987. Allochthonous terranes in the Andes of Ecuador and northwestern Peru. *Can. J. Earth Sci.* 24, 266–278.
- Ganne, J., Schellart, W., Rosenbaum, G., Feng, X., De Andrade, V., 2017. Probing crustal thickness evolution and geodynamic processes in the past from magma records: an integrated approach. *Geol. Soc. Am. Spec. Pap.* 526, 1–25.
- Garzzone, C.N., Hoke, G.D., Libarkin, J.C., Withers, S., MacFadden, B., Eiler, J., Ghosh, P., Mulch, A., 2008. Rise of the Andes. *Science* 320 (5881), 1304–1307.
- Gehrels, G.E., Valencia, V.A., Ruiz, J., 2008. Enhanced precision, accuracy, efficiency, and spatial resolution of U-Pb ages by laser ablation-multicollector-inductively coupled plasma-mass spectrometry. *Geochem. Geophys. Geosyst.* 9 (3) <https://doi.org/10.1029/2007GC001805>.
- Gonzalez, L., Clausen, B., Holk, G., Poma, O., 2020. Using Stable Isotopes to better understand the Petrologic and Hydrothermal Evolution of cretaceous Linga Complex of the Peruvian Coastal Batholith, near Ica. *Boletín de la Sociedad Geológica del Perú* 113, 12–25.
- Gregory, R.T., Criss, R.E., Taylor Jr., H.P., 1989. Oxygen isotope exchange kinetics of mineral pairs in closed and open systems: applications to problems of hydrothermal alteration of igneous rocks and Precambrian iron formations. *Chem. Geol.* 75 (1–2), 1–42.
- Gregory-Wodzicki, K.M., 2000. Uplift history of the Central and Northern Andes: a review. *GSA. Bulletin* 112 (7), 1091–1105.
- Gutscher, M.-A., 2002. Andean subduction styles and their effect on thermal structure and interplate coupling. *J. S. Am. Earth Sci.* 15, 3–10.
- Haederle, M., Atherton, M.P., 2002. Shape and Intrusion Style of the Coastal Batholith, vol. v. 345. *Tectonophysics, Peru*, pp. 17–28.
- Hanson, R.B., Sorensen, S.S., Barton, M.D., Fiske, R.S., 1993. Long-term evolution of fluid-rock interactions in magmatic arcs: evidence from the Ritter Range pendant, Sierra Nevada, California, and numerical modeling. *J. Petrol.* 34 (1), 23–62.
- Harrison, J.V., 1960. Geología de los alrededores de Baños en el Occidente del Perú Central. *Boletín de la Sociedad Geológica del Perú* 35, 63–77.
- Henrique-Pinto, R., Basei, M.A.S., Santos, P.R.D., Saad, A., Milani, E., Cingolani, C., Frugis, G.L., 2021. Paleozoic Paraná Basin transition from collisional retro-foreland to pericratonic syncline: Implications on the geodynamic model of Gondwana proto-Andean margin. *J. S. Am. Earth Sci.* 111 <https://doi.org/10.1016/j.jsames.2021.103511>.
- Hildebrand, R.S., Whalen, J.B., 2014. Arc and Slab-Failure Magmatism in Cordilleran Batholiths I – The Cretaceous Coastal Batholith of Peru and its Role in South American Orogenesis and Hemispheric Subduction. *Geosci. Can.* 41 (3), 255–282. <https://doi.org/10.12789/geocanj.2014.41.047>.
- Hildreth, W., Moorbath, S., 1988. Crustal contributions to arc magmatism in the Andes of Central Chile. *Contrib. Mineral. Petrol.* 98 (4), 455–489.
- Holk, G.J., Taylor, B.E., Galley, A.G., 2008. Oxygen isotope mapping of the Archeon Sturgeon Lake caldera complex and VMS-related hydrothermal system, Northwestern Ontario, Canada. *Mineral. Deposita* 43, 623–640.
- Hughes, G.R., Mahood, G.A., 2008. Tectonic controls on the nature of large silicic calderas in volcanic arcs. *Geology* 36 (8), 627–630.
- Isacks, B.L., 1988. Uplift of the central Andean plateau and bending of the Bolivian orocline. *J. Geophys. Res. Solid Earth* 93 (B4), 3211–3231.
- Ishikawa, T., Tera, F., 1999. Two isotopically distinct fluid components involved in the Mariana arc: evidence from Nb/B ratios and B, Sr, Nd, and Pb isotope systematics. *Geology* 27 (1), 83–86.
- Jaillard, E., Héral, G., Monfret, T., Díaz-Martínez, E., Baby, P., Lavenau, A., Dumont, J.F., 2000. Tectonic evolution of the Andes of Ecuador, Peru, Bolivia and northernmost Chile. In: Cordani, U.G., Milani, E.J., Thomaz Filho, A., Campos, D.A. (Eds.), *Tectonic evolution of South America*, pp. 481–559. Rio de Janeiro, Brazil.
- Jaillard, E., Soler, P., 1996. Cretaceous to early Paleogene tectonic evolution of the northern Central Andes (0–18°S) and its relations to geodynamics. *Tectonophysics* 259 (1–3), 41–53.
- James, D.E., 1971. Plate tectonic model for the evolution of the Central Andes. *Geol. Soc. Am. Bull.* 82 (12), 3325–3346.
- James, D.E., 1982. A combined O, Sr, Nd, and Pb isotopic and trace element study of crustal contamination in central Andean lavas, I. Local geochemical variations. *Earth Planet. Sci. Lett.* 57 (1), 47–62.
- Javoy, M., Fourcade, S., Allegre, C.J., 1970. Graphical method for examination of ¹⁸O/¹⁶O fractionations in silicate rocks. *Earth Planet. Sci. Lett.* 10, 12–16.
- Jenks, W.F., Harris, E.G., 1953. Plutonics near Arequipa as a petrologic sample of the coastal batholith of Peru. *Boletín de la Sociedad Geológica del Perú* 26, 79–94.
- Jiménez, N., López-Velásquez, S., 2008. Magmatism in the Huarina belt, Bolivia, and its geotectonic implications. *Tectonophysics* 459 (1), 85–106.
- Johnston, S., Gehrels, G., Valencia, V., Ruiz, J., 2009. Small-volume U–Pb zircon geochronology by laser ablation-multicollector-ICP-MS. *Chem. Geol.* 259 (3–4), 218–229.
- Jones, P.R., 1981. Crustal structures of the Peru continental margin and adjacent Nazca plate, 9°S latitude. In: Kulm, L.D., Dymond, J., Dasch, E.J., Hussong, D.M. (Eds.), *Nazca plate: Crustal formation and Andean convergence*, 154. Geological Society of America Memoir, pp. 423–443.
- Kaneoka, I., Guevara, C., 1984. K-Ar age determinations of late Tertiary and Quaternary Andean volcanic rocks, southern Peru. *Geochem. J.* 18 (5), 233–239.
- Kay, S.M., Coira, B., Viramonte, J., 1994. Young mafic back arc volcanic rocks as indicators of continental lithospheric delamination beneath the Argentine Puna plateau, Central Andes. *Journal of Geophysical Research: Solid Earth* 99 (B12), 24323–24339.

- Kay, S.M., Godoy, E., Kurtz, A., 2005. Episodic arc migration, crustal thickening, subduction erosion, and magmatism in the south-Central Andes. *Geol. Soc. Am. Bull.* 117 (1–2), 67–88.
- Kay, S.M., Mpodozis, C., Coira, B., 1999. Neogene magmatism, tectonism, and mineral deposits of the Central Andes (22°S to 33°S), in B. Skinner, ed. *Geology and mineral deposits of Central Andes*. Soc. Econ. Geol. 7, 27–59.
- Keppie, J.D., Ortega-Gutiérrez, F.J., 2010. 1.3–0.9 Ga Oaxaquia (Mexico): Remnant of an arc/backarc on the northern margin of Amazonia. *J. S. Am. Earth Sci.* 29 (1), 21–27.
- Keskin, M., 2013. AFC-Modeler: a Microsoft Excel Workbook Program for Modelling Assimilation combined with Fractional Crystallization (AFC) Process in Magmatic Systems by using Equations of DePaolo (1981). *Turk. J. Earth Sci.* 22 (2), 304–319.
- Kirsch, M., Paterson, S.R., Wobbe, F., Martínez-Ardila, A.M., Clausen, B.L., Alasino, P.H., 2016. Temporal histories of Cordilleran continental arcs: testing models for magmatic episodicity. *Am. Mineral.* 101 (10), 2133–2154.
- Kistler, R.W., Wooden, J.L., Premo, W.R., Morton, D.M., 2014. Pb-Sr-Nd-O isotopic characterization of Mesozoic rocks throughout the northern end of the Peninsular Ranges Batholith: Isotopic evidence for the magmatic evolution of oceanic arc-continental margin accretion during the late cretaceous of southern California. In: Morton, D.M., Miller, F.K. (Eds.), *Peninsular Ranges Batholith, Baja California and Southern California*, vol. 211. Geological Society of America Memoir, pp. 263–316.
- Lackey, J.S., Valley, J.W., Chen, J.H., Stockli, D.F., 2008. Dynamic magma systems, crustal recycling, and alteration in the Central Sierra Nevada Batholith: the oxygen isotope record. *J. Petrol.* 49, 1397–1426.
- Lipman, P.W., 2007. Incremental assembly and prolonged consolidation of Cordilleran magma chambers: evidence from the Southern Rocky Mountain volcanic field. *Geosphere* 3 (1), 42.
- Litherland, M., 1994. The metamorphic belts of Ecuador. *Overseas Mem Br Geol Surv v.* 11, 1–147.
- Loewy, S.L., Connelly, J.N., Dalziel, I.W.D., 2004. An orphaned basement block: the Arequipa-Antofalla Basement of the central Andean margin of South America. *Geol. Soc. Am. Bull.* 116 (1–2), 171–187.
- Ludwig, K., 2003. *User's Manual for Isoplot 3.00*. A Geochronological Toolkit for Microsoft Excel, vol. 4. Berkeley Geochronology Center Special Publication.
- Luffi, P., Ducea, M., 2022. Chemical mohometry: Assessing crustal thickness of ancient orogens using geochemical and isotopic data. *Rev. Geophys.* v. 60, no. 2 <https://doi.org/10.1029/2021RG000753>.
- Mamani-Huisa, M.-I., 2006. Variations in Magma Composition in Time and Space along the Central Andes (13° S–28° S): Göttingen Univ (Dissertation, 125p).
- Mamani, M., Tassara, A., Wörner, G., 2008. Composition and structural control of crustal domains in the Central Andes. *Geochem. Geophys. Geosyst.* 9 (3), Q03006. <https://doi.org/10.1029/2007GC001925>.
- Mamani, M., Wörner, G., Sempere, T., 2010. Geochemical variations in igneous rocks of the Central Andean orocline (13°S to 18°S): Tracing crustal thickening and magma generation through time and space. *Geol. Soc. Am. Bull.* 122 (1–2), 162–182.
- Martínez Ardila, A.M., Clausen, B.L., Memeti, V., Paterson, S.R., 2019a. Source contamination, crustal assimilation, and magmatic recycling during three flare-up events in the cretaceous Peruvian Coastal Batholith: an example from the Ica-Pisco plutons. *J. S. Am. Earth Sci.* 95 <https://doi.org/10.1016/j.jsames.2019.102300>.
- Martínez Ardila, A.M., Paterson, S.R., Memeti, V., Parada, M.A., Molina, P.G., 2019b. Mantle driven cretaceous flare-ups in Cordilleran arcs. *Lithos* 326, 19–27.
- Martínez Valladares, W., Cervantes Gárate, J., 2003. Rocas ígneas en el sur del Perú: nuevos datos geocronométricos, geoquímicos y estructurales entre los paralelos 16° y 18° 30' Latitud Sur. *Boletín D* 26, 140.
- Matthews, K.J., Seton, M., Müller, R.D., 2012. A global-scale plate reorganization event at 105–100 Ma. *Earth Planet. Sci. Lett.* 355, 283–298.
- Mégard, F., 1984. The Andean orogenic period and its major structures in central and northern Peru. *J. Geol. Soc.* 141 (5), 893–900.
- Mišković, A., Spikings, R.A., Chew, D.M., Košler, J., Ulianov, A., Schaltegger, U., 2009. Tectonomagmatic evolution of Western Amazonia: Geochemical characterization and zircon U-Pb geochronologic constraints from the Peruvian Eastern Cordilleran granitoids. *Geol. Soc. Am. Bull.* 121 (9–10), 1298–1324.
- Mitouard, P., Kissel, C., Laj, C., 1990. Post-Oligocene rotations in southern Ecuador and northern Peru and the formation of the Huancabamba deflection in the Andean Cordillera. *Earth Planet. Sci. Lett.* 98 (3–4), 329–339.
- Moore, N.D., 1979. The geology and geochronology of the Arequipa segment of the Coastal Batholith of Peru. University of Liverpool, dissertation, p. 549.
- Moore, N., Agar, R., 1985. Variations along a batholith: The Arequipa segment of the Coastal Batholith of Peru. In: Pitcher, W.S., et al. (Eds.), *Magmatism at a Plate Edge: The Peruvian Andes*. John Wiley, New York, pp. 108–118.
- Moore, N.D., 1984. Potassium-Argon ages from the Arequipa Segment of the Coastal Batholith of Peru and their correlation with regional tectonic events. *J. Geol. Soc.* 141 (3), 511–519.
- Mourier, T., 1988. La transition entre Andes marginales et Andes cordilleraïnes à ophiolites: évolution sédimentaire, magmatique et structurale du relais de Huancabamba (3 à 8 Lat: S; Nord Pérou-Sud Equateur): Paris, 11.
- Mpodozis, C., Ramos, V.A., 1989. The Andes of Chile and Argentina. In: Ericksen, G.E., et al. (Eds.), *Geology of the Andes and its Relation to Hydrocarbon and Mineral Resources*: Houston, Texas, Circum-Pacific Council for Energy and Mineral Resources Earth Science Series, pp. 59–90 vol. v. 11, ch. 5.
- Mukasa, S.B., 1984. Comparative Pb Isotope Systematics and Zircon U-Pb Geochronology for the Coastal, San Nicolas and Cordillera Blanca Batholiths, Peru. University of California, Santa Barbara dissertation (387 p).
- Mukasa, S.B., 1986. Common Pb isotopic compositions of the Lima, Arequipa and Toquepala segments in the Coastal batholith, Peru: Implications for magmagenesis. *Geochim. Cosmochim. Acta* 50, 771–782.
- Myers, J.S., 1975. Cauldron Subsidence and Fluidization: Mechanisms of Intrusion of the Coastal Batholith of Peru into its own Volcanic Ejecta. *Geol. Soc. Am. Bull.* 86 (9), 1209–1220.
- Noble, D.C., McKee, E.H., Megard, F., 1978. Eocene uplift and unroofing of the coastal batholith near Lima, central Peru. *J. Geol.* 86 (3), 403–405.
- Otamendi, J.E., Ducea, M.N., Tibaldi, A.M., Bergantz, G.W., de la Rosa, J.D., Vujovich, G. I., 2009. Generation of Tonalitic and Dioritic Magmas by coupled Partial Melting of Gabbroic and Metasedimentary Rocks within the Deep Crust of the Famatinian Magmatic Arc, Argentina. *J. Petrol.* 50 (5), 841–873.
- Pardo-Casas, F., Molnar, P., 1987. Relative motion of the Nazca (Farallon) and South American Plates since late cretaceous time. *Tectonics* 6 (3), 233–248.
- Paterson, S.R., Memeti, V., Mundil, R., Žák, J., 2016. Repeated, multiscale, magmatic erosion and recycling in an upper-crustal pluton: Implications for magma chamber dynamics and magma volume estimates. *Am. Mineral.* 101, 23.
- Paterson, S.R., Ducea, M.N., 2015. Arc magmatic tempos: gathering the evidence. *Elements* 11 (2), 91–98.
- Petford, N., Atherton, M.P., 1995. Crustal segmentation and the isotopic significance of the Abancay Deflection: Northern Central Andes (9–20° S): *Andean. Geology* 22 (2), 235–243.
- Pfiffner, O., Gonzalez, L., 2013. Mesozoic–Cenozoic Evolution of the Western Margin of South America: Case Study of the Peruvian Andes. *Geosciences* 3 (2), 262.
- Pitcher, W.S., Atherton, M.P., Cobbing, E.J., Beckinsale, R.D., 1985. *Magmatism at a Plate Edge: The Peruvian Andes*. Wiley.
- Plank, T., Cooper, L.B., Manning, C.E., 2009. Emerging geothermometers for estimating slab surface temperatures. *Nat. Geosci.* 2 (9), 611–615.
- Polliand, M., Schaltegger, U., Frank, M., Fontbote, L., 2005. Formation of intra-arc volcanosedimentary basins in the western flank of the central Peruvian Andes during Late Cretaceous oblique subduction: field evidence and constraints from U–Pb ages and Hf isotopes. *Int. J. Earth Sci.* 94, 231–242.
- Quang, C.X., Clark, A.H., Lee, W., Hawkes, N., 2005. Response of superegne processes to episodic Cenozoic uplift, pediment erosion, and ignimbrite eruption in the porphyry copper province of southern Peru. *Econ. Geol.* 100 (1), 87–114.
- Ramos, V., Alemán, A., 2000. Tectonic evolution of the Andes. In: Cordani, U.G., Milani, E.J., Filho, A. Thomaz, Campos, D.A. (Eds.), *Tectonic evolution of South America: 31st International Geological Congress, Rio de Janeiro*, pp. 635–685.
- Ramos, V.A., 1999. Plate tectonic setting of the Andean Cordillera. *Episodes J. Int. Geosci.* 22 (3), 183–190.
- Ramos, V.A., 2008. Patagonia: a Paleozoic continent adrift? *J. South Am. Earth Sci.* 26 (3), 235–251.
- Ramos, V.A., 2009. Anatomy and global context of the Andes: Main geologic features and the Andean orogenic cycle. In: Kay, S.M., Ramos, V.A., Dickinson, W.R. (Eds.), *Backbone of the Americas: Shallow Subduction, Plateau Uplift, and Ridge and Terrane Collision*: Geological Society of American Memoir, vol. 204, pp. 31–65.
- Ramos, V.A., 2010. The tectonic regime along the Andes: Present-day and Mesozoic regimes. *Geol. J.* 45 (1), 2–25.
- Ramos, V.A., 2018. Tectonic evolution of the Central Andes: From terrane accretion to crustal delamination. In: Zamora, G., McClay, K.M., Ramos, V.A. (Eds.), *Petroleum Basins and Hydrocarbon Potential of the Andes of Peru and Bolivia: AAPG Memoir*, vol. 117, pp. 1–34.
- Ramos, V.A., Folguera, A., 2005. Tectonic evolution of the Andes of Neuquén: constraints derived from the magmatic arc and foreland deformation. *Geol. Soc. London Spec. Publ.* 252 (1), 15–35.
- Regan, P.F., 1976. The Genesis and Emplacement of Mafic Plutonic Rocks of the Coastal Andean Batholith, Lima Province, Peru. University of Liverpool dissertation (186p).
- Regan, P.F., 1985. The early basic intrusions. In: Pitcher, W.S., et al. (Eds.), *Magmatism at a Plate Edge: The Peruvian Andes*. John Wiley, New York, pp. 72–89.
- Reimann, C.R., Bahlburg, H., Kooijman, E., Berndt, J., Gerdes, A., Carlotto, V., López, S., 2010. Geodynamic evolution of the early Paleozoic Western Gondwana margin 14°–17°S reflected by the detritus of the Devonian and Ordovician basins of southern Peru and northern Bolivia. *Gondwana Res.* 18 (2–3), 370–384.
- Reynolds, P.H., Dasch, E.J., 1971. Lead isotopes in marine manganese nodules and the ore-lead growth curve. *J. Geophys. Res.* 76 (21), 5124–5129.
- Rodriguez, J., Acosta, J., Castroviejo, R., Quispe, J., Romero, D., Uribe, R., Campian, M., 2010. Geología y estructura de las ultramafitas de Tapo y Acobamba (Tarma, Perú). *Removiliación tectónica Andina de un segmento ofiolítico Pre-Andino: XV Congreso Peruano de Geología*. In: *Resúmenes Extendidos*. Sociedad Geológica del Perú, Pub Esp., no. 9, pp. 79–82.
- Rodríguez Morante, I., Huanacuni Mamani, D., 2011. Síntesis geoeconómica de la región Piura: Instituto Geológico Minero y Metalúrgico del Perú "INGEMMET", pp. 79–82.
- Rogers, G., Hawkesworth, C.J., 1989. A geochemical traverse across the North Chilean Andes: evidence for crust generation from the mantle wedge. *Earth Planet. Sci. Lett.* 91 (3–4), 271–285.
- Rollinson, H., 1993. *Using Geochemical Data*. Longman, London (352p).
- Romero, D., Valencia, K., Alarcón, P., Peña, D., Ramos, V.A., 2013. The offshore basement of Perú: evidence for different igneous and metamorphic domains in the forearc. *J. S. Am. Earth Sci.* 42, 47–60.
- Romero Fernández, D., Valencia, K., Alarcón, P., Ramos, V., 2011. Geología de la costa pacífica del Perú central entre Chiclayo y Paracas (7 214 sur). In: *Proceedings Memorias 14th Congreso Latinoamericano de Geología and 13th Congreso Colombiano de Geología*, Medellín, pp. 110–111.
- Romeuf, N., Münch, P., Soler, P., Jaillard, E., Pik, R., Aguirre, L., 1997. Mise en évidence de deux lignées magmatiques dans le volcanisme du Jurassique inférieur de la zone subandine équatorienne: *Comptes Rendus-Académie des Sciences Paris serie 2 Sciences de la Terre et des Planètes Fascicule A*, v. 324, pp. 361–368.

- Sanchez-Fernandez, A.W., 1982. Edades Rb-Sr en los segmentos Arequipa-Toquepala del Batolito de la costa del Peru, Quinto Congreso Latinoamericano de Geología: Argentina, pp. 487–504.
- Santos, A., Weimin, G., Tassinari, C., Soberon, D., Ccallo, W., 2016. Geocronología U-Pb sobre zircones en la contrastación de la evolución espacial-temporal del magmatismo y la metalogenia del Batolito de la Costa “segmento Arequipa”. In: Proceedings XVIII Congreso Peruano de Geología, pp. 1–7.
- Schellart, W.P., 2017. Andean mountain building and magmatic arc migration driven by subduction-induced whole mantle flow. *Nat. Commun.* 8 (1), 2010.
- Schmitz, M., 1994. A balanced model of the southern Central Andes. *Tectonics* 13 (2), 484–492.
- Schwartz, J.J., Klepeis, K.A., Sadowski, J.F., Stowell, H.H., Tulloch, A.J., Coble, M.A., 2017. The tempo of continental arc construction in the Mesozoic median Batholith, Fiordland, New Zealand. *Lithosphere* 9 (3), 343–365.
- Sdrolias, M., Müller, R.D., 2006. Controls on back-arc basin formation. *Geochem. Geophys. Geosyst.* v. 7, no. 4 <https://doi.org/10.1029/2005GC001090>.
- Sébrier, M., Mercier, J.L., Macharé, J., Bonnot, D., Cabrera, J., Blanc, J.L., 1988. The state of stress in an overriding plate situated above a flat slab: the Andes of Central Peru. *Tectonics* 7 (4), 895–928.
- Sempere, T., Carlier, G., Soler, P., Fornari, M., Carlotto, V.C., Jacay, J., Arispe, O., Néraudeau, D., Cárdenas, J., Rosas, S., Jiménez, N., 2002. Late Permian–Middle Jurassic lithospheric thinning in Peru and Bolivia, and its bearing on Andean-age tectonics. *Tectonophysics* 345 (1–4), 153–181.
- Sempere, T., Folguera, A., Gerbault, M., 2008. New insights into Andean evolution: an introduction to contributions from the 6th ISAG symposium (Barcelona, 2005). *Tectonophysics* 459 (1). <https://doi.org/10.1016/j.tecto.2008.03.011>.
- Shackleton, R., Ries, A., Coward, M., Cobbold, P.R., 1979. Structure, metamorphism and geochronology of the Arequipa Massif of coastal Peru. *J. Geol. Soc.* 136 (2), 195–214.
- Sharp, Z.D., 1990. A laser-based microanalytical method for the *in situ* determination of oxygen isotope ratios of silicates and oxides. *Geochim. Cosmochim. Acta* 54, 1353–1357.
- Soler, P., Bonhomme, M.G., 1990. Relation of magmatic activity to plate dynamics in Central Peru from late cretaceous to present. In: Kay, S.M., Rapela, C.W. (Eds.), *Plutonism from Antarctica to Alaska: Geological Society of America Special Paper*, 241, pp. 173–192.
- Stern, T.W., Bateman, P.C., Morgan, B.A., Newell, M.F., Peck, D.L., 1981. Isotopic U-Pb Ages of Zircon from the Granitoids of the Central Sierra Nevada, California. USGS Professional Paper, 1185.
- Stewart, J., Garcia, W., 1968. Geología de los cuadrangulos de Mollendo y La Joya. *Boletín del Servicio Geológico Minero del Perú* 19 (19), 1–93.
- Stewart, J.W., Evernden, J.F., Snelling, N.J., 1974. Age determinations from Andean Peru: a reconnaissance survey. *Geol. Soc. Am. Bull.* 85 (7), 1107–1116.
- Stracke, A., et al., 2003. Recycling oceanic crust: Quantitative constraints. *Geochem. Geophys. Geosyst.* 4 (3), 14–33.
- Swenson, J.L., Beck, S.L., Zandt, G., 2000. Crustal structure of the Altiplano from broadband regional waveform modeling: implications for the composition of thick continental crust. *J. Geophys. Res. Solid Earth* 105 (B1), 607–621.
- Taylor Jr., H.P., Sheppard, S.M.F., 1986. Igneous rocks: I. Processes of isotopic fractionation and isotope systematics. In: Valley, J.W., Taylor Jr., H.P., O’Neil, J.R. (Eds.), *Stable Isotopes in High Temperature Geological Processes. Reviews in Mineralogy*, 16, pp. 227–272.
- Taylor, W.P., 1973. The Geochemistry and Mineralogy of Cañas and Puscao Plutons, Lima Province. Peru. University of Liverpool dissertation (196p).
- Timoteo, D., Romero, D., Valencia, K.J.L., 2012. Posible existencia de la Faja Alleghanide? en el Noroeste del Perú: Recientes dataciones Ar/Ar y U-Pb, e implicancias en un Sistema Petrolero de la Cuenca Talara: Sociedad Geológica del Perú, 16th Congreso Peruano de Geología.
- Tosdal, R., Farrar, E., Clark, A.H., 1981. K-Ar geochronology of the late Cenozoic volcanic rocks of the Cordillera Occidental, southernmost Peru. *J. Volcanol. Geotherm. Res.* 10 (1–3), 157–173.
- Trumbull, R.B., Riller, U., Oncken, O., Scheuber, E., Munier, K., Hongn, F.D., 2006. The time-space distribution of Cenozoic volcanism in the South-Central Andes: a new data compilation and some tectonic implications. *Andes Active Subduction Orogeny* 29–43. https://doi.org/10.1007/978-3-540-48684-8_2.
- Turner, S.J., Langmuir, C.H., 2015. The global chemical systematics of arc front stratovolcanoes: evaluating the role of crustal processes. *Earth Planet. Sci. Lett.* 422, 182–193.
- Vidal C. C.E., Injoque-Espinoza, J., Sidder, G.B., Mukasa, S.B., 1990. Amphibolitic Cu-Fe skarn deposits in the central coast of Peru. *Econ. Geol.* 85 (7), 1447–1461.
- Villagomez, R., Jaillard, E., Bulot, L., Rivadeneira, M., Vera, R., 1996. The Aptian-late Albian marine transgression in the oriente basin of Ecuador. In: *International Symposium on Andean Geodynamics*, 3rd, St. Malo, France, 1996, Proceedings, pp. 521–524.
- Voos, A., Martínez-Ardila, A.M., Clausen, B.L., 2021. Zircon ages reveal unexpected older flare-up in the Peruvian Coastal Batholith. *GSA Cordilleran Online Section* 53.
- Willner, A.P., Tassinari, C.C., Rodrigues, J.F., Acosta, J., Castroviejo, R., Rivera, M., 2014. Contrasting Ordovician high- and low-pressure metamorphism related to a microcontinent-arc collision in the Eastern Cordillera of Perú (Tarma province). *J. S. Am. Earth Sci.* 54, 71–81.
- Winter, L.S., 2008. The Genesis of “Giant” Copper-Zinc-Gold-Silver Volcanogenic Massive Sulphide Deposits at Tambogrande, Perú : Age, Tectonic Setting, Paleomorphology, Lithochemistry, and Radiogenic Isotopes [Doctor of Philosophy - PhD: University of British Columbia] (274 p).
- Wipf, M.A., 2006. Evolution of the Western Cordillera and Coastal Margin of Peru: Evidence from Low-Temperature Thermochronology and Geomorphology. Ph.D. thesis. Swiss Fed. Inst. of Technol, Zürich, Switzerland, pp. 14–18.
- Wise, J., 2002. Examples of syntectonic emplacement instead of passive pluton emplacement in the Coastal Batholith of Peru and implications for late Cretaceous Nazca plate motions. *Boletín de la Sociedad Geológica del Perú* 94, 99–106.
- Witt, C., Rivadeneira, M., Poujol, M., Barba, D., Beida, D., Beseme, G., Montenegro, G., 2017. Tracking ancient magmatism and Cenozoic topographic growth within the Northern Andes forearc: Constraints from detrital U-Pb zircon ages. *Geol. Soc. Am. Bull.* 129 (3–4), 415–428.
- Wörner, G., Lezaun, J., Beck, A., Heber, V., Lucassen, F., Zingg, E., Rössling, R., Wilke, H.G., 2000. Precambrian and early Paleozoic evolution of the Andean basement at Belén (northern Chile) and Cerro Uyarani (western Bolivia Altiplano). *J. S. Am. Earth Sci.* 13 (8), 717–737.
- Zelasco, L.D.N., 2011. Tectonic Evolution of the Contaya Arch Ucyali Basin, Peru. MsC Thesis. Graduate Studies of Texas A&M University, p. 57.
- Zellmer, G.F., 2008. Some first-order observations on magma transfer from mantle wedge to upper crust at volcanic arcs: Geological Society. *Lond. Special Publ.* 304 (1), 15–31.
- Zheng, Y.F., 1993. Calculation of oxygen isotope fractionation in hydroxyl-bearing silicates. *Earth Planet. Sci. Lett.* 120 (3–4), 247–263.